

A flexible model for correlated count data, with application to multi-condition differential expression analyses of single-cell RNA sequencing data

Yusha Liu¹, Peter Carbonetto^{2,3}, Michihiro Takahama^{4,5}, Adam Gruenbaum⁶, Dongyue Xie⁷, Nicolas Chevrier⁴, and Matthew Stephens^{*2,7}

¹Department of Biostatistics, The University of North Carolina at Chapel Hill, Chapel Hill, NC, USA

²Department of Human Genetics, The University of Chicago, Chicago, IL, USA

³Research Computing Center, The University of Chicago, Chicago, IL, USA

⁴Pritzker School of Molecular Engineering, The University of Chicago, Chicago, IL, USA

⁵Graduate School of Pharmaceutical Sciences, Osaka University, Osaka, Japan

⁶Institute for Health Metrics and Evaluation, University of Washington, Seattle, WA, USA

⁷Department of Statistics, The University of Chicago, Chicago, IL, USA

Abstract

Detecting differences in gene expression is an important part of single-cell RNA sequencing experiments, and many statistical methods have been developed for this aim. Most differential expression analyses focus on comparing expression between two groups (e.g., treatment vs. control). But there is increasing interest in *multi-condition differential expression analyses* in which expression is measured in many conditions and the aim is to accurately detect and estimate expression differences in all conditions. We show that directly modeling single-cell RNA-seq counts in all conditions simultaneously, while also inferring how expression differences are shared across conditions, leads to greatly improved performance for detecting and estimating expression differences compared to existing methods. We illustrate the potential of this new approach by analyzing data from a single-cell experiment studying the effects of cytokine stimulation on gene expression. We call our new method “Poisson multivariate adaptive shrinkage”, and it is implemented in an R package available at <https://github.com/stephenslab/poisson.mash.alpha>.

1 Introduction

Detecting differences in gene expression — that is, “differential expression” (DE) analysis — has been a fundamental analysis aim ever since the introduction of technologies to measure gene expression (Soneson and Delorenzi, 2013). As measurement technologies have improved, gene expression data sets have increased in size and resolution, bringing new analysis challenges. The development of RNA sequencing (RNA-seq) technologies (Wang et al., 2009) has greatly facilitated the measurement of gene expression in “bulk” samples. More recently, the development of single-cell RNA sequencing technologies (scRNA-seq) has allowed for rapid, high-throughput measurement of gene

*mstephens@uchicago.edu

expression in individual cells, resulting in large datasets profiling gene expression in thousands of cells (e.g., [Zheng et al., 2017](#)).

Increasingly, biologists are developing scRNA-seq experiments in which gene expression is assayed *in many experimental conditions*. For example, in the motivating data set for this paper, gene expression data were obtained for approximately 142,000 cells under 45 different treatment conditions. In *multi-condition data* such as these, we seek to understand which changes in expression are specific to certain conditions (“condition-specific effects”), and which changes are shared among two or more conditions (“shared effects”). In this paper, we develop methods to tackle these aims — specifically, to detect which genes are differentially expressed, and to estimate the log-fold changes (LFCs) *among multiple conditions*. While many methods exist for performing differential expression analysis of scRNA-seq data, analyzing multi-condition scRNA-seq data raises at least two key challenges that are not adequately addressed by existing methods.

First, when assessing expression across multiple conditions, many different patterns of differential expression are possible. For example, some genes may be differentially expressed in a single condition (relative to all other conditions), while other genes may show similar expression differences in subsets of conditions. Typically, these patterns are unknown in advance, but one would like to identify and exploit them to improve accuracy of the LFC estimates, and to improve power to detect differentially expressed genes. To address this first challenge, we build on the empirical Bayes (EB) method developed in [Urbut et al. \(2019\)](#), “multivariate adaptive shrinkage” (“mash” for short), which is designed to model and adapt to effect-sharing patterns among conditions present in the data.

Second, the data from scRNA-seq experiments are molecular counts, which are most naturally modeled using count models such as Poisson measurement models ([Townes et al., 2019](#); [Sarkar and Stephens, 2021](#)). However, there is no straightforward way to integrate a Poisson model with mash because the Poisson model does not naturally provide summary statistics — effect estimates and standard errors — that can be used by mash; in particular, estimates of standard errors are unreliable in Poisson models ([Robinson and Smyth, 2008](#)). An alternative would be to combine mash with a Gaussian measurement model for *log-transformed* scRNA-seq counts (e.g., [Finak et al., 2015](#)). However, as has been repeatedly pointed out (e.g., [Lun, 2018](#); [Townes et al., 2019](#); [Crowell et al., 2020](#)), this data transformation can lead to severe bias in the LFC estimates. This is particularly an issue when many of the counts are zero or small, *which is a common feature of scRNA-seq data sets*. This suggests that it would be desirable to combine mash with a model of the scRNA-seq counts.

Therefore, to get the best of both worlds — improved accuracy achieved by exploiting patterns of effect-sharing across conditions and the advantages of directly modeling the scRNA-seq counts without first transforming them — we pursue an approach that *models the scRNA-seq count data jointly in all conditions*. We call this new approach “Poisson mash” because it is based on a Poisson model of the data, and, like mash, it improves accuracy in the effect estimates by flexibly modeling the sharing of effects across conditions. Since the gains in accuracy will be greater as more conditions with shared effects are included in the analysis, in this paper we focus on scRNA-seq experiments in which gene expression is measured in many (e.g., dozens) conditions. Although its development has been motivated by our interest in analyzing multi-condition scRNA-seq data sets, the Poisson mash model can also be viewed as a general model of multivariate count data, so the ideas contained in this paper may be useful in other settings where multivariate count data occur.

The structure of the paper is as follows. First, in [Section 2](#), we define “multi-condition differ-

ential expression analysis” more formally, and explain the underlying assumptions about the data. Next, we introduce the core Poisson mash model (Section 3), discuss related methods (Section 4), then describe several enhancements to the model that improve its performance in more realistic settings (Section 5). In Section 6, we evaluate the benefits of Poisson mash approach compared with existing methods in simulated scRNA-seq data sets. To illustrate how Poisson mash can be used to gain biological insights from multi-condition gene expression data, we apply Poisson mash to the scRNA-seq data set mentioned above (Section 7). Finally, we wrap up with a discussion (Section 8).

1.1 Software availability

The Poisson mash methods are implemented in the R package “poisson.mash.alpha”, which is available at <https://github.com/stephenslab/poisson.mash.alpha>.

2 Problem setup

In a *multi-condition differential expression analysis*, the aim is to compare expression for each of J genes across R conditions from multi-condition count data \mathbf{X} ,

$$\mathbf{X} = \begin{matrix} & \begin{matrix} x_{11} & x_{12} & \cdots & x_{1R} \\ x_{21} & x_{22} & \cdots & x_{2R} \\ \vdots & \vdots & \ddots & \vdots \\ x_{J1} & x_{J2} & \cdots & x_{JR} \end{matrix} \\ \begin{matrix} J \\ \text{genes} \end{matrix} & \left[\right. & & & \left. \right] \\ & & \begin{matrix} R \\ \text{conditions} \end{matrix} & & \end{matrix} \quad (2.1)$$

This matrix can be obtained by summing, for each gene j , the unique molecular identifier (UMI) counts from all cells in the same condition (see Section 2.1). The special case of $R = 2$ — that is, when \mathbf{X} is a $J \times 2$ matrix — corresponds to the standard setup for DE analysis in which the aim is to compare expression between two conditions (e.g., treatment vs. control). By contrast, we focus on *multi-condition experiments with $R \gg 2$* ; for example, in the cytokines data, $R = 45$.

Next, we assume a *Poisson measurement model* for the counts,

$$x_{jr} \sim \text{Pois}(s_r \lambda_{jr}), \quad (2.2)$$

independently for each gene j and condition r , in which $s_r > 0$ denotes a “size factor”.¹ The parameter λ_{jr} in (2.2) represents a relative rate, specifically the *relative expression level* for gene j in condition r .

To analyze differences in expression, the log-relative expression is decomposed into a baseline level of expression, μ_j , and a condition-specific expression difference β_{jr} relative to the baseline:

$$\log \lambda_{jr} = \mu_j + \beta_{jr}. \quad (2.3)$$

Our main aim is to accurately estimate the expression differences β_{jr} and other statistical quantities

¹In DE analyses of scRNA-seq data, the size factors s_r are often defined as the sum of the counts in each condition, $s_r = \sum_{j=1}^J x_{jr}$. This is the default setting for our analyses, noting that other definitions are possible (e.g., Bullard et al., 2010).

involving β_{jr} . With these modeling assumptions, the μ_j and β_{jr} are not individually identifiable from the count data, \mathbf{X} . However, they become identifiable once one introduces priors for β_{jr} ; this is described in the next section where we introduce the Poisson mash model.

The assumption that the data are in the form of a $J \times R$ matrix \mathbf{X} implies that there is only a *single independent observation per condition*. This assumption is not critical; when multiple replicates are available per condition, we can aggregate cells by replicate rather than by condition so that there are multiple independent observations per condition. This extension is described in Appendix C. But the single-observation assumption simplifies the description of the method, and furthermore the extension to multiple observations is not essential for understanding of the method nor appreciating its benefits.

2.1 Obtaining \mathbf{X} from multi-condition scRNA-seq data

In multi-condition scRNA-seq data, we observe the UMI counts y_{ji} for genes $j \in \{1, \dots, J\}$ in cells $i \in \{1, \dots, N\}$ in which each cell i is measured in one of R conditions. To analyze the differences in expression across R conditions following the setup described above, we summarize the UMI counts in each condition by summing them across cells from the same condition; that is, for each gene j and condition r , we set $x_{jr} = \sum_{i \in \mathcal{S}_r} y_{ji}$, where $\mathcal{S}_r \subset \{1, \dots, N\}$ denotes the indices of the cells that are measured in condition r .

The idea of summing the UMI counts from the individual cells is commonly described as “pseudobulk analysis”, and its benefits were noted in several recent papers (Lun and Marioni, 2017; Ahlmann-Eltze and Huber, 2020; Erdmann-Pham et al., 2021; Murphy and Skene, 2022; Crowell et al., 2020; Squair et al., 2021). In the context of multi-condition DE analysis, forming pseudobulk data has the twin advantages of simplifying modeling and reducing computation, and for these reasons we take this approach here. One possible concern with a pseudobulk analysis of single-cell RNA-seq data is that one may need to correct for unwanted variation (known or unknown) that must be accounted for at the single-cell level (Risso et al., 2014; Leek and Storey, 2007; Leek, 2014; Gerard and Stephens, 2020). We address this concern in Section 5.2.

3 The basic Poisson mash model

We now give the minimum details needed to understand Poisson mash. Enhancements to the basic model are described in Section 5.

3.1 The multivariate adaptive shrinkage prior

Our main aim is to detect and estimate expression differences among conditions. For example, if some subset of conditions involves treatments with similar biological effects, then the expression differences β_{jr} are expected to be similar to one another; on the other hand, if one treatment has a very different biological effect from other treatments, it may show a “condition-specific” effect in which β_{jr} is nonzero only in that condition. Furthermore, the patterns of DE may vary across genes; for example, genes in the same pathway may show more similar patterns of DE than genes in different pathways. In summary, different data sets will likely exhibit different patterns of DE among conditions, and multiple patterns of DE may be present within a single data set.

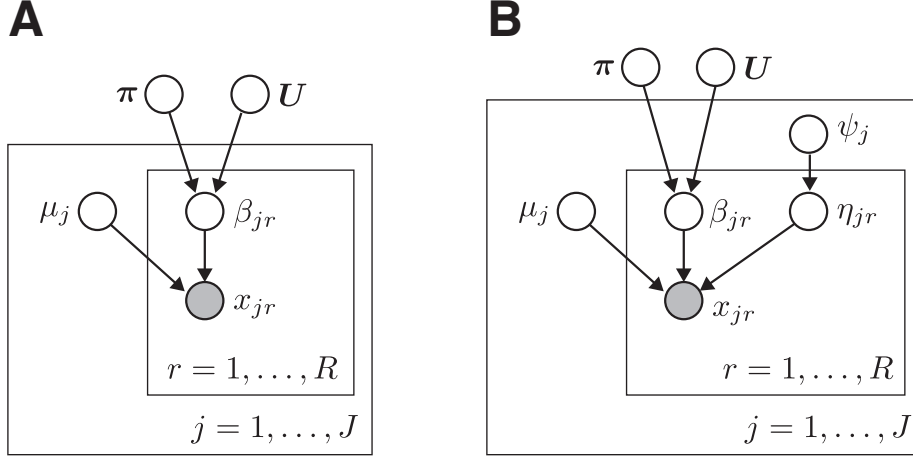


Figure 1: Directed acyclic graphs (DAGs) showing the independence structure of the basic Poisson mash model (A) and the Poisson mash model augmented with random effects (B).

To capture heterogeneous DE patterns, and adapt these patterns to the data, we use the multivariate adaptive shrinkage (“mash”) prior introduced in [Urbut et al. \(2019\)](#),

$$p(\boldsymbol{\beta}_j; \boldsymbol{\pi}, \mathbf{U}) = \sum_{k=1}^K \sum_{l=1}^L \pi_{kl} N_R(\boldsymbol{\beta}_j; \mathbf{0}, w_l \mathbf{U}_k), \quad (3.1)$$

where $\boldsymbol{\beta}_j := (\beta_{j1}, \dots, \beta_{jR})'$, and $N_R(\cdot; \boldsymbol{\mu}, \boldsymbol{\Sigma})$ denotes the density of the R -variate normal distribution with mean $\boldsymbol{\mu}$ and covariance matrix $\boldsymbol{\Sigma}$. Here, $w_l > 0, l = 1, \dots, L$, is a pre-specified “grid” of scaling coefficients, spanning from very small to very large, to capture the full range of possible effect sizes, and the π_{kl} are mixture weights, $\pi_{kl} \geq 0$, $\sum_{k=1}^K \sum_{l=1}^L \pi_{kl} = 1$. Each \mathbf{U}_k is an $R \times R$ covariance matrix that captures a pattern of covariation of effects across conditions. We refer to the Poisson measurement model (2.2–2.3) together with the mash prior (3.1) as “Poisson mash”. The graphical model representation of the Poisson mash model is shown in Panel A of Figure 1.

The covariance matrices \mathbf{U}_k can include both pre-specified “canonical” covariance matrices that represent, for example, DE specific to a condition, and “data-driven” covariance matrices that are estimated from the data, and can capture arbitrary patterns of DE among the conditions. Each weight π_{kl} should capture the relative frequency of each combination of scaling coefficient w_l and cross-condition pattern \mathbf{U}_k . These weights will be estimated from the data.

The mash prior (3.1) is centered on zero, which helps address the nonidentifiability of μ_j and β_{jr} in (2.3); specifically, centering the prior on zero encourages the average β_{jr} to be near zero, and is analogous to the (non-Bayesian) approach of identifying parameters by imposing the constraint $\sum_{r=1}^R \beta_{jr} = 0$. In addition, we note that typically the prior will place considerable weight near zero, reflecting the fact that many expression differences are zero or small. This has the effect of “shrinking” many of the estimated β_{jr} towards zero.

Our model is closely connected to multivariate Poisson log-normal (MPLN) distributions, originally proposed by [Aitchison and Ho \(1989\)](#) as a flexible approach to modeling dependencies among Poisson variables. Indeed, integrating out the effects $\boldsymbol{\beta}_j$, the marginal distribution of the counts for gene j , $\mathbf{x}_j := (x_{j1}, \dots, x_{jR})'$, is a mixture of MPLNs. Similar MPLN mixture models have recently

been used to cluster multivariate count measurements in biological applications (Silva et al., 2019; Subedi and Browne, 2020).

3.2 Inference aims

With the Poisson mash model, we focus on the following types of inferences:

Inference Aim 1: Detect differentially expressed genes Test the “global null” hypothesis of no DE for gene j , $H_{0j}: \beta_{jr} = 0 \forall r$.

Inference Aim 2: Detect and estimate expression differences relative to a reference condition When a single condition serves as the control condition, we detect and estimate changes in each condition r relative to the control condition, and quantify uncertainty in these estimates, say, by reporting interval estimates. For example, supposing condition 1 is the control, then $\log(\lambda_{jr}/\lambda_{j1}) = \beta_{jr} - \beta_{j1}$ is the log-fold change in condition $r \geq 2$ relative to the control.²

Not all experiments have a single natural reference or control condition. In such cases, one could estimate changes in condition r relative to the mean or median across all conditions: $\beta_{jr} - \text{mean}\{\beta_{j1}, \dots, \beta_{jR}\}$ or $\beta_{jr} - \text{median}\{\beta_{j1}, \dots, \beta_{jR}\}$. The median may be preferable to the mean in situations when a few conditions are very different from the others. For example, suppose the expression of gene j is upregulated in condition r only. In this example, the deviation of β_{jr} from the median will be nonzero (and positive) only in condition r , whereas its deviation from the mean will be positive in condition r and negative (and smaller in magnitude) in all other conditions.

3.3 Variational empirical Bayes algorithm

We take the same empirical Bayes (EB) approach in mash (Urbut et al., 2019). This involves two key computations:

- (i) Estimate the mash prior — specifically, the prior covariances $\mathbf{U} := \{\mathbf{U}_1, \dots, \mathbf{U}_K\}$ and the mixture weights $\boldsymbol{\pi}$ — by pooling information from the J genes.
- (ii) Compute gene-specific posterior quantities using the prior estimated in (i).

A major difference between mash and Poisson mash is that mash is based on a Gaussian measurement model, and therefore benefits from the convenient analytical properties of mixtures of multivariate Gaussians, whereas Poisson mash is based on a Poisson measurement model that does not result in analytic posterior computations. Therefore, some approximations must be made to obtain computations that are analytic and tractable. We propose to use variational approximation techniques (Blei et al., 2017) to obtain fast posterior computations. Specifically, we use the Gaussian variational approximation described by Arridge et al. (2018). With this approximation, the exact

²The convention in DE analysis, originating from DE analyses in microarray experiments, is to use the base-2 logarithm. In all our results, we report LFC estimates and related quantities using the base-2 logarithm.

posterior distribution of β_j ,

$$\begin{aligned} p_{\text{post}}(\beta_j) &:= p(\beta_j \mid \mathbf{x}_j, \mu_j, \boldsymbol{\pi}, \mathbf{U}) \\ &\propto p(\mathbf{x}_j \mid \beta_j, \mu_j) p(\beta_j; \boldsymbol{\pi}, \mathbf{U}) \\ &\propto p(\mathbf{x}_j \mid \beta_j, \mu_j) \times \sum_{k=1}^K \sum_{l=1}^L \pi_{kl} N_R(\beta_j; \mathbf{0}, w_l \mathbf{U}_k), \end{aligned} \quad (3.2)$$

which does not have an analytic formula, is approximated by a mixture of multivariate Gaussian distributions,

$$p_{\text{post}}(\beta_j) \approx q_j(\beta_j) := \sum_{k=1}^K \sum_{l=1}^L \zeta_{jkl} N_R(\beta_j; \boldsymbol{\varphi}_{jkl}, \boldsymbol{\Sigma}_{jkl}). \quad (3.3)$$

That is, q_j acts as the approximate posterior for β_j . The idea behind the variational inference approach is to search for the free parameters $\zeta_{jkl}, \boldsymbol{\varphi}_{jkl}, \boldsymbol{\Sigma}_{jkl}, k = 1, \dots, K, l = 1, \dots, L$, that produce a q_j which most closely resembles the true posterior distribution of β_j . This parameter search is most frequently done using numerical optimization techniques. That is, when we describe fitting the approximate posterior distribution q_j , we are actually optimizing the parameters $\zeta_{jkl}, \boldsymbol{\varphi}_{jkl}, \boldsymbol{\Sigma}_{jkl}$.

To develop algorithms for mixture models, such as EM algorithms, a common data augmentation trick is to introduce a latent variable that indicates the source mixture component. For each gene j , we define a latent indicator $z_{jkl} \in \{0, 1\}$ that is 1 if β_j is drawn from mixture component (j, k) , and zero otherwise. With this data augmentation, we have

$$\beta_j \mid z_{jkl} = 1 \sim N_R(\mathbf{0}, w_l \mathbf{U}_k), \quad (3.4)$$

and the approximate posterior is defined as

$$q_j(\beta_j, \mathbf{z}_j) = \prod_{k=1}^K \prod_{l=1}^L \{\zeta_{jkl} N_R(\beta_j; \boldsymbol{\varphi}_{jkl}, \boldsymbol{\Sigma}_{jkl})\}^{z_{jkl}}. \quad (3.5)$$

This definition recovers (3.3) after marginalizing over \mathbf{z}_j .

The algorithm for fitting the variational approximation proceeds by maximizing a lower bound to the likelihood, sometimes called the ‘‘evidence lower bound’’, or ELBO (Blei et al., 2017). Since the likelihood naturally factorizes over the genes, the ELBO in turn is a simple sum,

$$\text{ELBO}(q_1, \dots, q_J; \boldsymbol{\mu}, \boldsymbol{\pi}, \mathbf{U}) = \sum_{j=1}^J \text{ELBO}_j(q_j; \mu_j, \boldsymbol{\pi}, \mathbf{U}), \quad (3.6)$$

in which the ELBO for gene j is

$$\text{ELBO}_j(q_j; \mu_j, \boldsymbol{\pi}, \mathbf{U}) := \log p(\mathbf{x}_j \mid \mu_j, \boldsymbol{\pi}, \mathbf{U}) - D_{\text{KL}}(q_j(\beta_j, \mathbf{z}_j) \parallel p_{\text{post}}(\beta_j, \mathbf{z}_j)), \quad (3.7)$$

where $D_{\text{KL}}(q \parallel p)$ denotes the Kullback-Leibler (KL) divergence from q to p (Cover and Thomas, 2006). While both terms on the right-hand side of (3.7) are intractable, the intractable parts will cancel out in the expression for the ELBO, which leads to tractable computations under the approximation (3.3). See Appendix E for detailed derivations.

To maximize the ELBO (3.6), we take an “EM-like” co-ordinate ascent approach, in which we alternate between maximizing the ELBO with respect to the approximate posteriors q_1, \dots, q_J (the “E step”), and maximizing the ELBO with respect to the model parameters $\boldsymbol{\mu}, \boldsymbol{\pi}, \boldsymbol{U}$ (the “M step”), until some convergence criterion is met, yielding parameter estimates $\hat{\boldsymbol{\mu}}, \hat{\boldsymbol{\pi}}, \hat{\boldsymbol{U}}$ and approximate posteriors $\hat{q}_1, \dots, \hat{q}_J$. This co-ordinate ascent algorithm resembles an EM algorithm except that the E step produces approximate posterior expectations, and for this reason this algorithm is sometimes called “variational EM” (Blei et al., 2017). Note that the M step in this algorithm pools the information across all J genes to estimate the parameters, whereas the posterior computations in the E step are independent for each gene j and therefore can be performed in parallel. For more details on this, see Appendix E.

3.4 Posterior statistics

Now we define the posterior quantities that we use to tackle the inference aims, and we briefly explain how they are computed.

We estimate expression differences and quantify their uncertainty (Inference Aim 2) using the approximate posteriors $\hat{q}_j(\boldsymbol{\beta}_j)$. Since the approximate posteriors are mixtures of multivariate normals, posterior means and covariances of $\boldsymbol{\beta}_j$ are available analytically, and other posterior quantities can be computed by Monte Carlo simulation. In particular, we estimate the LFC relative to a control (assumed without loss of generality to be condition 1) as simply the posterior expectation $\mathbb{E}[\beta_{jr} - \beta_{j1}] = \mathbb{E}[\beta_{jr}] - \mathbb{E}[\beta_{j1}]$, in which these expectations are taken with respect to the approximate posterior \hat{q}_j . When the LFC is defined relative to the median expression level, we compute a Monte Carlo estimate by simulating from \hat{q}_j .

To determine whether an expression difference is significant (Inference Aim 2), we use the *local false sign rate* (*lfsr*) (Stephens, 2017),

$$lfsr_{jr} := \min \{ \Pr(\beta_{jr} \geq 0), \Pr(\beta_{jr} \leq 0) \}, \quad (3.8)$$

in which the probabilities $\Pr(\beta_{jr} \geq 0)$ and $\Pr(\beta_{jr} \leq 0)$ are again obtained from \hat{q}_j . The *lfsr* is a measure of significance that is analogous to local false discovery rate (*lfdr*) but more conservative since it controls the probability that the sign of β_{jr} is incorrectly estimated rather than the probability that β_{jr} is incorrectly called nonzero (given the observed data). The *lfsr* was also found to be more robust to modeling assumptions than the *lfdr* (Stephens, 2017).

The *lfsr* (3.8) defines a *condition-specific* measure of significance; to tackle Inference Aim 1, we need to define a *gene-level* measure of significance. To this end, we propose the *minimum lfsr*,

$$min\text{-}lfsr_j := \min \{ lfsr_{j1}, \dots, lfsr_{jR} \}. \quad (3.9)$$

Gene j is considered to be a differentially expressed gene if $min\text{-}lfsr_j < \alpha$, and is considered to be differentially expressed in condition r if $lfsr_{jr} < \alpha$, for some $\alpha \in (0, 1)$. The *lfsr* threshold α controls the stringency of the tests and is chosen by the analyst; in this paper, we use $\alpha = 0.05$ unless stated otherwise.

We note that a simpler alternative to the *minimum lfsr* is to compute a *Bayes factor* for $\boldsymbol{\beta}_j \neq \mathbf{0}$ vs. $\boldsymbol{\beta}_j = \mathbf{0}$,

$$BF_j := \frac{p(\mathbf{x}_j \mid \hat{\boldsymbol{\mu}}_j, \hat{\boldsymbol{\pi}}, \hat{\boldsymbol{U}})}{p(\mathbf{x}_j \mid \hat{\boldsymbol{\mu}}_j^{\text{null}}, \boldsymbol{\beta}_j = \mathbf{0})},$$

where $\hat{\mu}_j^{\text{null}}$ is an estimate of μ_j under the null model. In practice, the numerator in the Bayes factor is difficult to compute and therefore we approximate it by the ELBO, $\log p(\mathbf{x}_j | \hat{\mu}_j, \hat{\boldsymbol{\pi}}, \hat{\mathbf{U}}) \approx \text{ELBO}_j(\hat{q}_j; \hat{\mu}_j, \hat{\boldsymbol{\pi}}, \hat{\mathbf{U}})$. The ELBO is a lower bound, so the approximate Bayes factor will always be an underestimate of the exact Bayes factor, resulting in more conservative detection of DE genes. In our initial evaluations, we found that the Bayes factor did not perform as well as the *minimum lfsr*, perhaps due to the approximation used in our calculation of the Bayes factors, so we recommend using the *minimum lfsr* for a gene-level measure of significance.

We also implemented a test to assess the goodness-of-fit for a Poisson mash model; the details are given in Appendix D.

4 Related work

Many statistical methods are available to perform multi-condition DE analysis of scRNA-seq data. Extensive reviews and comparisons of these methods have been conducted (Soneson and Robinson, 2018; Wang et al., 2019) and we refer the reader to these papers for details on the available methods. Among the variety of DE analysis methods, widely used methods include limma (Law et al., 2014; Smyth, 2004), MAST (Finak et al., 2015), edgeR (Robinson et al., 2010) and DESeq2 (Anders and Huber, 2010; Love et al., 2014; Zhu et al., 2019). While limma, edgeR and DESeq2 were originally developed respectively for microarray expression data and bulk RNA-seq data, they have also been found to work well for scRNA-seq data (Soneson and Robinson, 2018). MAST, by contrast, was specifically designed to cope with the particulars of scRNA-seq data. None of these methods share the ability of Poisson mash to combine information across conditions.

MultiDE (Kang et al., 2016) and CorMotif (Wei et al., 2015), which were developed with bulk RNA-seq data in mind, share some of the features of Poisson mash. Among the two, MultiDE is more like Poisson mash. Like Poisson mash, MultiDE is aimed at performing DE analysis jointly over multiple conditions. MultiDE models RNA-seq counts y_{ji} using the negative binomial (NB) distribution; for $i \in \mathcal{S}_r, y_{ji} \sim \text{NB}(\mu_{jr}, \phi_j)$, in which j indexes genes, r indexes conditions and i indexes replicates. A key difference is that MultiDE makes a restrictive assumption about how expression differences are shared across conditions. Specifically, MultiDE assumes $\log \mu_{jr} = \mu_j + u_r v_j$. Therefore, MultiDE can be viewed as a special case of the Poisson mash model in which the mash prior (3.1) has a single component ($K = 1$), and a single covariance matrix, $\mathbf{U}_1 = \mathbf{u}\mathbf{u}'$, where $\mathbf{u} = (u_1, \dots, u_R)'$. MultiDE is not expected to perform well when these prior assumptions are violated.

CorMotif is intended for comparing differences in expression between two groups in multiple independent studies (or conditions, or cell-types, etc.). A similar setup is also considered in a recent benchmarking paper assessing methods for differential expression analysis (Crowell et al., 2020). However, this setup is quite different from our setup where we have a single observation in each of the many conditions, and our aim is to compare gene expression across conditions. Additionally, in contrast with Poisson mash, CorMotif focuses on DE detection, and not on estimation of the effect sizes (log-fold changes), and CorMotif does not directly model the counts. Despite these differences, CorMotif shares with Poisson mash the idea of modeling shared patterns of DE across multiple studies (they call these patterns “correlation motifs”), and using these shared patterns to increase power of DE detection.

5 Enhancements to the basic Poisson mash model

In this section, we describe two important practical improvements to the basic Poisson mash model: (i) a “random effect” to account for additional sources of experimental variation; and (ii) latent factors to account for “unwanted variation” that can induce dependence among the gene-level tests. (In the remainder of this paper, the random effect enhancement is included in all applications of the method unless stated otherwise.)

5.1 Modeling random effects

Even in the absence of expression differences ($\beta_{jr} = 0$ for all $r = 1, \dots, R$), there might be heterogeneity in λ_{jr} across conditions due to other sources of experimental variation. To account for this variation, we introduce a “random effect” η_{jr} ,

$$\log \lambda_{jr} = \mu_j + \beta_{jr} + \eta_{jr}, \quad (5.1)$$

and assign a normal prior to the random effects for each gene,

$$\boldsymbol{\eta}_j \sim N_R(\mathbf{0}, \psi_j^2 \mathbf{I}_R), \quad (5.2)$$

where $\boldsymbol{\eta}_j := (\eta_{j1}, \dots, \eta_{jR})'$, ψ_j^2 is an unknown, gene-specific parameter to be estimated from the data, and \mathbf{I}_R is the $R \times R$ identity matrix. The basic model (2.3) is recovered from this model by setting $\psi_j^2 = 0$. Panel B of Figure 1 shows the graphical model for Poisson mash with random effects.

Based solely on the Poisson likelihood, only the sum $\beta_{jr} + \eta_{jr}$ is identifiable, not the individual terms in this sum. The different priors are what make it possible to simultaneously estimate both the expression differences β_{jr} and the random effects η_{jr} ; the prior for $\boldsymbol{\eta}_j$ is independent across conditions, whereas the prior for $\boldsymbol{\beta}_j$ is not. Therefore, correlations across conditions are explained only by the expression differences β_{jr} and not by the random effects η_{jr} . In addition, because η_{jr} has an identical normal prior in all conditions, the model may prefer to explain a strong condition-specific effect in condition r using β_{jr} rather than η_{jr} .

The addition of the random effect in (5.1) can be seen as an alternative to the negative binomial model (as used by edgeR and DESeq2, as well as other methods for analyzing RNA-seq data) to allow for greater flexibility in modeling variation in the counts. In particular, by integrating out $\boldsymbol{\eta}_j$, x_{jr} is marginally modeled by a *Poisson-log normal distribution*. The mean and variance of the counts under this model are

$$\begin{aligned} \mathbb{E}[x_{jr}] &= s_r e^{\mu_j + \beta_{jr} + \psi_j^2/2} \\ \text{Var}[x_{jr}] &= \mathbb{E}[x_{jr}] \times \{1 + \mathbb{E}[x_{jr}](e^{\psi_j^2} - 1)\}. \end{aligned}$$

It is easy to see from these expressions that ψ_j^2 affects the level of overdispersion for gene j , and in particular, when $\psi_j^2 = 0$ there is no overdispersion; that is, $\mathbb{E}[x_{jr}] = \text{Var}[x_{jr}]$, recovering the property of the Poisson that its mean and variance are the same.

We note that the Poisson log-normal model was used in Gu et al. (2014) to model inter-sample variation for DE analysis of RNA-seq data.

5.2 Correcting for unwanted variation

We further extend the Poisson mash model to allow for the incorporation of D additional variables $\boldsymbol{\rho}_d := (\rho_{1d}, \dots, \rho_{Rd})'$, $d = 1, \dots, D$. These variables represent sources of unwanted variation present in the data that can induce dependence among gene-wise tests and confound DE analysis (Leek and Storey, 2007; Leek, 2014). The augmented model is

$$\log \lambda_{jr} = \mu_j + \beta_{jr} + \eta_{jr} + \sum_{d=1}^D f_{jd} \rho_{rd}, \quad (5.3)$$

in which the f_{jd} are the regression coefficients for the confounding variables. Let \mathbf{F} denote the $J \times D$ matrix with elements f_{jd} , and let $\boldsymbol{\rho}$ denote the $R \times D$ matrix with elements ρ_{rd} . We assume \mathbf{F} has been previously estimated from the cell-level data \mathbf{Y} , and is therefore treated as “known” when fitting the Poisson mash model, whereas $\boldsymbol{\rho}$ will be estimated along with the other parameters of the Poisson mash model.

Because the primary motivation for including these additional variables is to correct for unwanted variation, we call this augmented model “Poisson mash RUV”, where the “RUV” is short for “removing unwanted variation”. In our experiments (Section 6), we compare Poisson mash with and without the RUV enhancement — that is, the models based on the two different definitions of the Poisson rates λ_{jr} in (5.1) and in (5.3) — to show how correcting for unwanted variation improves detection of expression differences.

In some cases, the confounding variables are known, such as when these capture batch effects. More often, the unwanted variation is due to unmeasured factors, in which case these variables can be estimated using one of the several methods developed for this aim, such as RUVSeq (Risso et al., 2014), svaseq (Leek and Storey, 2007; Leek, 2014) or mouthwash (Gerard and Stephens, 2020). (The best method to use may depend on the specifics of the RNA-seq experiment, e.g., whether negative controls are available.) Regardless of the specific method used, \mathbf{X} alone cannot be used to estimate the unknown confounders. When the cell-level data \mathbf{Y} are available, it is reasonable to estimate \mathbf{F} from \mathbf{Y} , then use the same \mathbf{F} for Poisson mash (for justification, see Appendix A).

In our analyses, we estimated \mathbf{F} by fitting a GLM-PCA model (Townes et al., 2019) with D factors to the single-cell data (the UMI counts) \mathbf{Y} . To avoid learning factors that correspond to the conditions, we included the condition labels as covariates in the GLM-PCA model. After fitting the GLM-PCA model, we took \mathbf{F} to be the \mathbf{V} matrix from the GLM-PCA model fit (following the notation of Townes et al. 2019).

6 Simulations

We performed simulations to evaluate Poisson mash and compare with other DE analysis approaches.

Most comparisons of DE analysis methods have focused on evaluating their ability to detect differentially expressed genes (e.g., Squair et al. 2021; Sonesson and Robinson 2018; Wang et al. 2019), i.e., how accurately a method is able to correctly identify the genes that are differentially expressed. In the multi-condition setting where the gene might show differences in expression in one or more conditions, the corresponding question is how well the method can correctly identify

the genes that are differentially expressed in *at least one condition* (Inference Aim 1). However, it is also of interest to identify the specific condition, or conditions, that give rise to differences in expression; in other words, identifying the *gene-condition pairs* with differences in expression (Inference Aim 2). We therefore evaluated the performance of the methods in achieving both of these aims. We also assessed accuracy of the expression difference estimates.

6.1 Simulation design

We simulated data sets by applying “binomial thinning” (Gerard, 2020) to the scRNA-seq data set described in Section 7 and in more detail in the Appendix. Binomial thinning is a technique intended to preserve as much as possible the properties of real scRNA-seq data.

The original scRNA-seq data contained UMI counts in different cell subpopulations, but to simplify the simulations we focused on the largest subpopulation, the B cells (Supplementary Table S1). For our simulations, we used cells from 25 of the 45 treatment conditions. Note that the amount of expression data was fairly even across all conditions (Supplementary Data).

Like most scRNA-seq data sets, the UMI counts were sparse; 93% of the UMI counts were zero. Also, like most scRNA-seq data sets, the average expression rates of the genes varied greatly; the top 1% of genes by expression level had a median UMI count of 4.4 per cell, whereas the median UMI count per cell across all genes was 0.02. The sequencing depths (total UMI counts) also varied widely across cells; they ranged from 500 to 20,000, with a median of 1,800. These aspects are handled naturally by the Poisson mash model and other Poisson-based models, whereas other models (e.g., limma, MAST) typically require careful preprocessing (log-transformation and normalization) of the data to account for these features.

From these data, we generated a smaller data set and a larger data set. For the smaller data set, we selected $N = 2,096$ cells uniformly at random from the 25 treatment conditions. For the larger data set, we randomly selected $N = 15,705$ cells from the same 25 conditions. In both data sets, we filtered out genes expressed in fewer than 25 cells. After this filtering step, the small data set contained $J = 8,358$ genes and the large data set contained $J = 10,691$ genes.

Next, starting with either the small or large data set, we took the following steps to simulate data sets.

First, we generated “null” data by randomly shuffling the treatment labels among the cells. This eliminated systematic differences in expression among treatments. Importantly, we shuffled the treatment labels in the same way for all genes. This preserves correlations among the genes that could confound the detection of expression differences; this same approach was used in Gerard and Stephens (2020). Note that any random effects that might have been specific to some treatment conditions were evened out across conditions by the random shuffling procedure.

After creating the null data, we used binomial thinning to add treatment effects to some genes, independently of the unwanted variation in the data. Once a treatment effect was chosen, binomial thinning involved simulating new counts from a binomial distribution *conditioned on the original counts*. To illustrate, consider the simpler case of two conditions. In this case, simulating an increase in expression of gene j in condition 2 relative to condition 1 — that is, $\beta_{j2} > 0$ — involved simulating a “thinned” count for each cell i in condition 1 as $y_{ji}^{\text{new}} \sim \text{Binomial}(y_{ji}, e^{-\beta_{j2}})$. Gerard (2020) explains how this idea is extended to more than two conditions.

In the smaller data sets, we added treatment effects in this way to 600 out of the 8,358 genes chosen uniformly at random from the subset of genes with a total UMI count of at least 200. In the larger data sets, we added treatment effects to 1,000 genes chosen uniformly at random

among the genes with a total UMI count of at least 229. For each selected gene j , we simulated the effect vector as $\beta_j = (\beta_{j1}, \dots, \beta_{jR})'$ for the $R = 25$ treatment conditions from $\beta_j = a_j w_j \mathbf{u}_j$, where the sign $a_j \in \{-1, +1\}$ was -1 or $+1$ with equal probability, w_j was drawn uniformly at random from $[\log 1.5, \log 5]$, and $\mathbf{u}_j \in \mathbb{R}^{25}$ was drawn uniformly at random from three sharing patterns (Supplementary Figure S1): the first sharing pattern simulated the situation in which only a single treatment condition (condition 21) had differences in expression; and the second and third sharing patterns simulated the situation in which the differences in expression were shared among subsets of treatments (conditions 9–11 and 12–19, respectively). Note that several of the conditions — conditions 1–8, 20 and 22–25 — were “null” conditions in that there were no gene expression differences in *any* of the simulations for these conditions. We arbitrarily treated the first treatment condition as the control, and LFCs were defined with respect to this control condition. Since the the largest u_{jr} was always 1, this produced fold changes that were at most 5 in magnitude (or the LFCs that were at most $\log_2 5 \approx 2.3$ in magnitude). Under these settings, many of the true effects β_{jr} were small enough that there would be a benefit to pooling information across multiple conditions.

We repeated this procedure 20 times for the large data set and another 20 times for the small data set to produce a total of 40 simulated data sets.

6.2 Methods compared

We compared two variants of Poisson mash — Poisson mash with and without the “RUV” enhancement — and several alternative methods that have been published and have good software implementations. (Both variants of Poisson mash included the “random effect” enhancement.)

The method most comparable to Poisson mash is mash (Urbut et al., 2019). mash takes as input a $J \times R$ matrix of condition-level expression estimates and another $J \times R$ matrix containing the standard errors of these estimates. We ran limma (Smyth, 2004) to generate these matrices.

To assess the benefits of mash and Poisson mash over methods that cannot exploit sharing of expression differences across conditions, we also compared with standard DE analysis methods. Specifically, we included three DE analysis methods — limma (Smyth, 2004), edgeR (Robinson et al., 2010) and MAST (Finak et al., 2015) — which were among the best-performing methods in the Sonesson and Robinson (2018) benchmarking study. These three methods (as well as other widely used DE analysis methods) effectively make the assumption that *expression differences are independent across conditions*.

We also included the nonparametric Kruskal-Wallis test in our comparisons (Kruskal and Wallis, 1952). Although the rank-based Kruskal-Wallis test is not frequently used for DE analysis, it is often used in other settings to detect differences among multiple groups, and therefore it is natural to compare mash and Poisson mash with the Kruskal-Wallis test. A benefit of the Kruskal-Wallis test is that it is nonparametric and therefore should be less sensitive to modeling assumptions. On the other hand, a disadvantage of the Kruskal-Wallis test is that it does not provide condition-level results, therefore we only used it for Inference Aim 1.

An important yet under-appreciated aspect of DE analysis of scRNA-seq data is that accounting for unwanted variation can substantially improve accuracy. (Although this aspect seems to have been neglected from many benchmarking studies, several methods have been developed to fill this need; e.g., Risso et al. 2014; Leek 2014; Gerard and Stephens 2020.) Therefore, to assess the benefits of accounting for unwanted variation, we compared Poisson mash with and without the additional terms capturing unwanted variation.

See Appendix F for details on how the methods were applied to the simulated data sets.

A fundamental difference between Poisson mash and the other methods is that Poisson mash works with the aggregated (“pseudobulk”) data, \mathbf{X} , whereas the other methods work with the cell-level data \mathbf{Y} , or a transformed version of \mathbf{Y} . The benefits and drawbacks of a pseudobulk analysis have been studied elsewhere (Lun and Marioni, 2017; Ahlmann-Eltze and Huber, 2020; Crowell et al., 2020; Squair et al., 2021), and assessing and understanding them remains an active research question. Since our principal aim is to evaluate Poisson mash and compare against alternatives, and not to study the benefits of pseudobulk analysis, we have tried to design the simulations so that there should be no particular benefit to analyzing \mathbf{X} instead of \mathbf{Y} . However, since Poisson mash and the other methods are based on different models, and are estimating different parameters, it is difficult to separate the benefits of analyzing \mathbf{X} vs. \mathbf{Y} from other aspects.

6.3 Performance evaluation

To evaluate the methods in the simulations, we used the following performance metrics.

For Inference Aim 1 (“detect differentially expressed genes”), the true differentially expressed genes were defined simply as the genes j for which $\beta_{jr} \neq 0$ in at least one condition r . (Recall, we have defined the LFC with respect to the first condition, and in the simulated data sets β_{j1} was always zero.) We then summarized performance using power and false discovery rate (FDR) as the p -value or $lfsr$ threshold for reporting DE genes was varied from 0 to 1. Power and false discovery rate (FDR) were calculated as $\text{FDR} := \frac{\text{FP}}{\text{TP} + \text{FP}}$ and $\text{power} := \frac{\text{TP}}{\text{TP} + \text{FN}}$, where FP, TP, FN, TN denote the number of false positives, true positives, false negatives and true negatives, respectively.

For Inference Aim 2, we evaluated detection and estimation of expression differences, again relative to the control condition. We defined the true differentially expressed gene-condition pairs as all pairs (j, r) , $r > 1$, such that $\beta_{jr} \neq 0$, then we calculated power and FDR for this task. Following Urbut et al. (2019), we only considered a gene-condition pair to be a true positive if the p -value or $lfsr$ met the threshold and if the sign of β_{jr} was correctly estimated.

To evaluate the accuracy of the LFC estimates, we calculated the root mean squared error $\text{RMSE} := \sqrt{\text{MSE}}$ for a specified subset of genes G as

$$\text{MSE} := \frac{1}{|G| \times (R - 1)} \sum_{j \in G} \sum_{r=2}^R [(\hat{\beta}_{jr} - \hat{\beta}_{j1}) - (\beta_{jr} - \beta_{j1})]^2.$$

6.4 Simulation results

First, we compared the methods’ ability to detect DE genes and condition-level expression differences. These comparisons are summarized in Figure 2, Panels A, B, D and E. These plots show power and FDR for each method as the p -value threshold (for edgeR, MAST, limma and Kruskal-Wallis) or $lfsr$ threshold (for mash and Poisson mash) is varied. As expected, the methods typically performed better in the larger data sets. Compared to edgeR, MAST, limma and the Kruskal-Wallis test, which do not model effect sharing across conditions, mash, Poisson mash and Poisson mash RUV achieved much greater power in both the small and large data sets. (The Kruskal-Wallis does not provide condition-level inferences so cannot compete this task.) The performance gains are particularly striking for detecting condition-level expression changes (B, E).

Next, we compared the methods’ ability to estimate the condition-level expression differences. Summarizing the estimation accuracy of LFCs by gene expression level (Figure 2, Panels C and F),

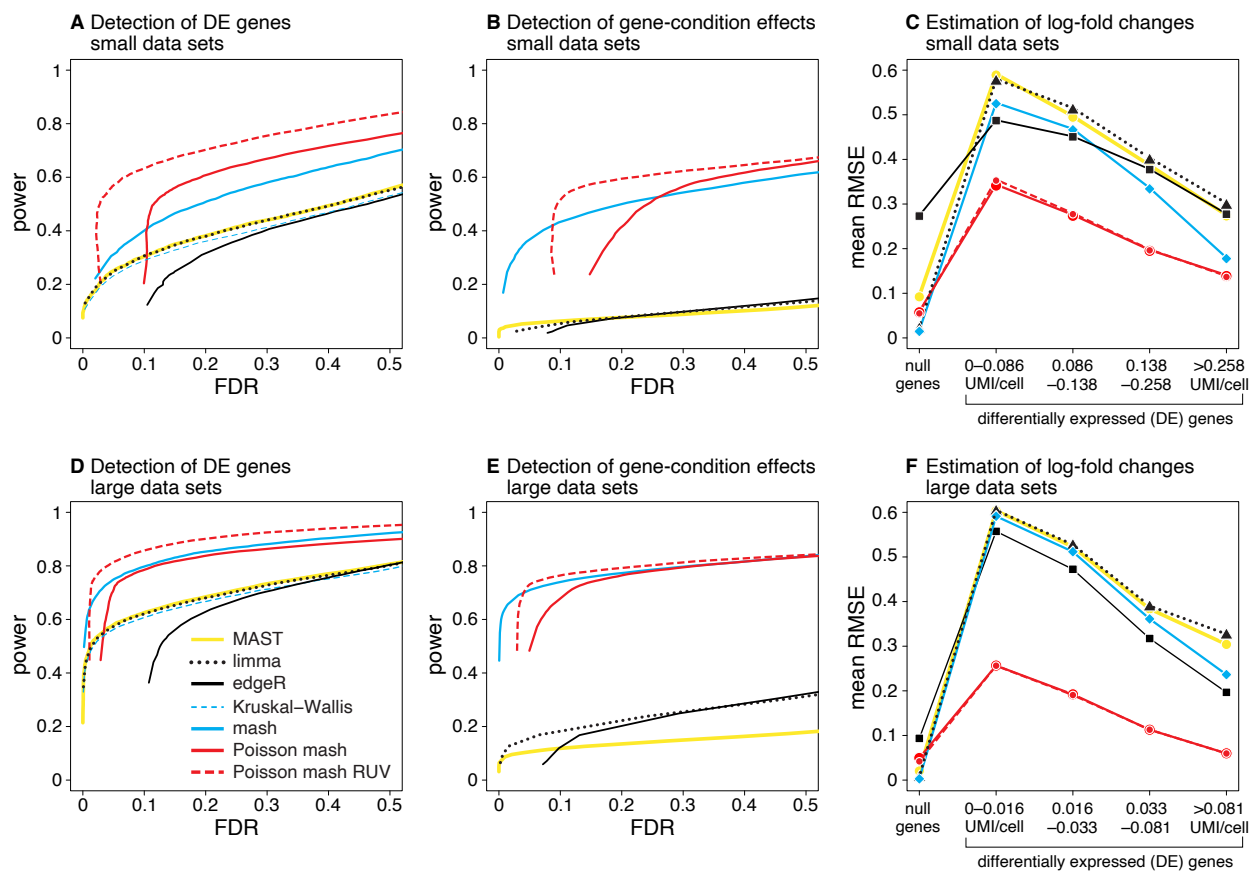


Figure 2: Evaluation of DE analysis methods in the small (top row) and large (bottom row) simulated data sets. FDR and power were calculated for all genes (A, D) and for all gene-condition pairs (B, E) in the 20 simulations by varying a p -value or $lfsr$ threshold from 0 to 1. Panels C and F summarize LFC estimation accuracy by the RMSE, averaged over 20 simulations. RMSE was calculated in non-overlapping sets of genes: “null” genes (genes in which there were no differences in expression in all conditions); and DE genes grouped by expression level (counts of UMIs per cell). Note that the Kruskal-Wallis method was only included in A and D because it does not provide condition-level inferences.

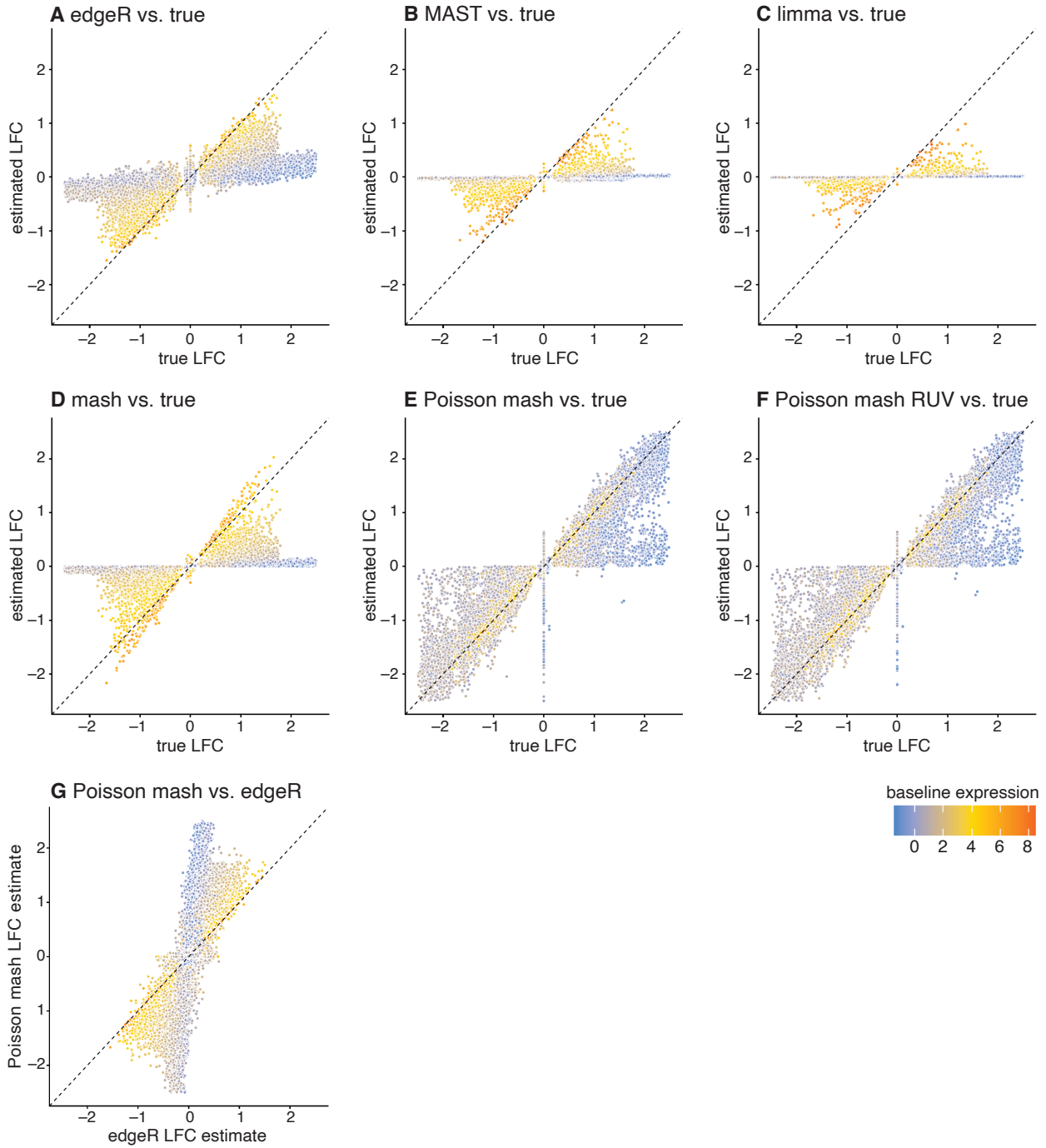


Figure 3: More detailed evaluation of LFC estimation accuracy. Each scatterplot shows the true LFC against the estimated LFC (in log base-2), except for the scatterplot at the bottom, which compares the edgeR and Poisson mash estimates. Each point depicts a result for a gene-condition pair (j, r) . DE genes are shown only from 5 of the large simulated data sets, so each scatterplot shows results for $5 \times 1,000 \times 24 = 120,000$ gene-condition pairs. Note that most true β_{jr} values are zero, even for DE genes, because a minority of conditions have differences in expression. The Kruskal-Wallis method is not included in these results because it does not provide condition-level estimates. All points are colored by the baseline expression level, μ_j , that was estimated by Poisson mash RUV.

Poisson mash and Poisson mash RUV had by far the best accuracy at all expression levels, with the greatest gains for genes at lower expression levels.

To understand these performance gains in greater detail, in Figure 3 we compared the true LFCs $\beta_{jr} - \beta_{j1}$ versus the estimated LFCs $\hat{\beta}_{jr} - \hat{\beta}_{j1}$. MAST and limma usually underestimated the LFCs, except for the most highly expressed genes. Since mash was provided with the limma estimates as input, mash also suffered from the same underestimation issue, although it was able to improve accuracy for effects that were shared across conditions. Similar to mash, Poisson mash also improved accuracy of the effect estimates but, unlike mash, Poisson mash was not disadvantaged by the poor initial estimates provided by limma. As a result, Poisson mash was often very accurate even for lowly expressed genes.

Since limma and MAST and, by extension, mash, work with log-transformed counts, whereas Poisson mash works with the “raw” counts, a key question is to what extent we should attribute these improvements to (i) combining of information across conditions using the flexible mash priors and (ii) to the use of a Poisson model of the counts instead of a Gaussian model of the log-transformed counts. (The log-transformation introduces biases in the LFC estimates, and this bias remains regardless of the choice of pseudocount used in the log-transformation; see Supplementary Figure S2.) To help answer this question, we compared Poisson mash to edgeR, which is also based on a Poisson model of the counts. The results of running edgeR show that while the underestimation problem is not quite as severe in edgeR, the overall pattern is similar to MAST and limma; for all three methods, the LFCs were estimated accurately mainly for highly expressed genes only. Only after combining the Poisson model with informative mash priors did we improve accuracy in lowly expressed genes as well.

Despite the fact that Poisson mash was much more accurate than mash, surprisingly this improvement did not necessarily translate to an improvement in power, particularly at lower false discovery rates — compare mash to Poisson mash in Panels A, B, D and E in Figure 2. Poisson mash provides improvements in power *only after* including additional factors in the model to account for unwanted variation, i.e., Poisson mash RUV. Poisson mash RUV does not noticeably increase accuracy of the LFC estimates over Poisson mash (Figure 2, Panels C and F), but it substantially improves the ability of Poisson mash to detect DE genes and condition-level expression differences (Figure 2, Panels A, B, D, E). Poisson mash RUV is only worse than mash at low FDRs. It is possible that improvements to estimation of the overdispersion parameters ψ_j^2 and unwanted variation coefficients f_{jd} — say, by adaptively shrinking these parameters jointly across all genes j (Love et al., 2014; Robinson et al., 2010) — may close the gap between mash and Poisson mash RUV at low FDRs. Despite this one limitation, the simulations show that Poisson mash RUV provides the best overall combination of (i) strong performance in detecting expression differences and (ii) accurate estimation of these differences.

6.5 Simulations with fewer conditions

Although we expect Poisson mash to be most beneficial in multi-condition data sets with many conditions, it is also of interest to know whether Poisson mash can cope with a smaller number of conditions. Therefore, we performed additional simulations with $R = 6$ and $R = 12$ conditions. We simulated 20 $R = 6$ data sets and another 20 $R = 12$ data sets, similar to above, with the following changes: the $R = 6$ data sets had $J = 9,160$ genes and $N = 3,898$ cells; the $R = 12$ data sets had $J = 10,003$ genes and $N = 7,960$ cells; in each data set, 1,000 of the genes were chosen uniformly at random to have treatment effects, and the non-null effects were generated from

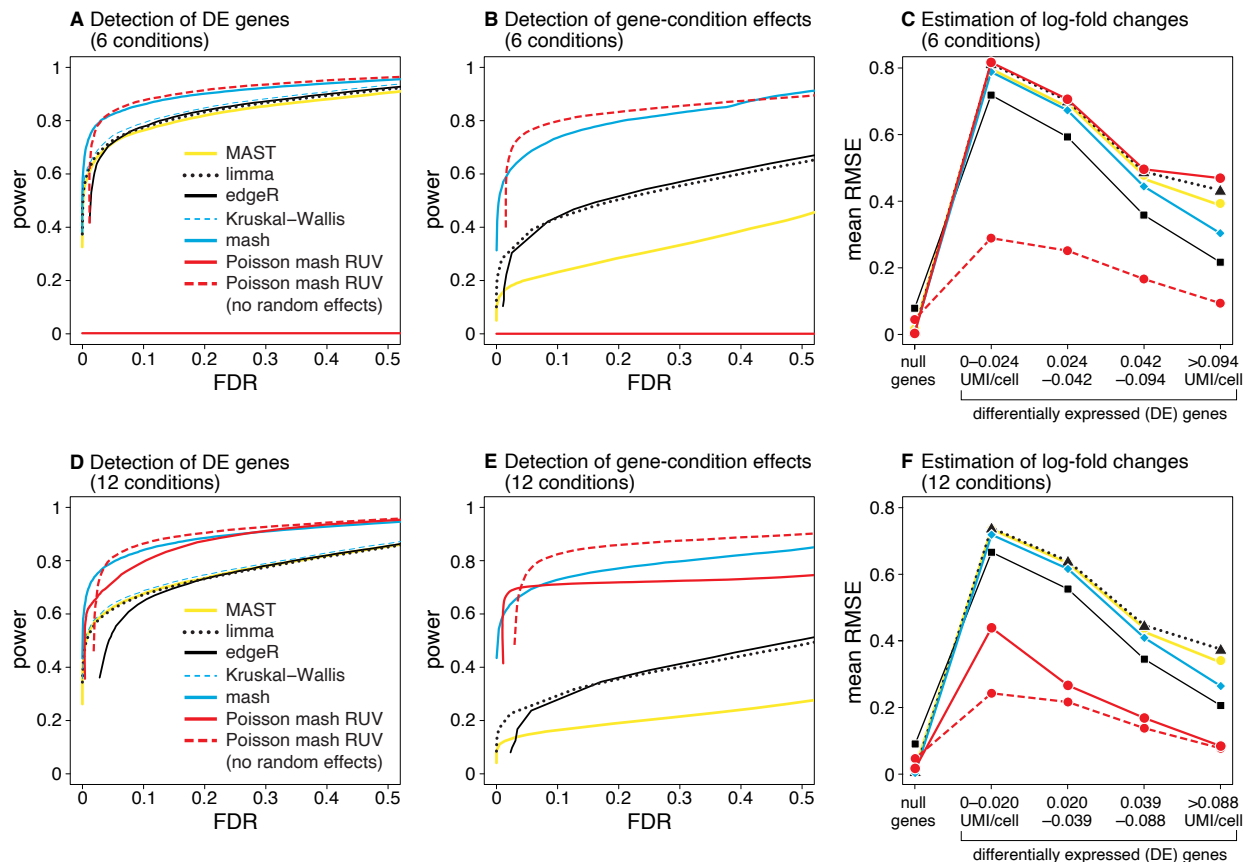


Figure 4: Evaluation of DE analysis methods in simulated data sets with fewer conditions. FDR and power were calculated for all genes (A, D) and for all gene-condition pairs (B, E) in the 20 simulations by varying a p -value or $lfsr$ threshold from 0 to 1. Panels C and F summarize LFC estimation accuracy by the RMSE, averaged over 20 simulations. RMSE was calculated in non-overlapping groups of genes: “null” genes (genes in which there were no differences in expression in all conditions); and DE genes grouped by expression level (counts of UMIs per cell). The results of the Kruskal-Wallis method are only included in Panels A and D because this method does not provide condition-level inferences.

one of two effect-sharing patterns: a condition-specific effect and an effect shared among multiple conditions (Supplementary Figure S1).

The results of these simulations are summarized in Figure 4. While Poisson mash RUV still maintained good performance with 12 conditions, it performed poorly in the data sets with only 6 conditions. In particular, at a *minimum* $lfsr$ threshold of 0.05, Poisson mash RUV identified an average of 571 DE genes in the $R = 12$ data sets, but an average of only 0.2 DE genes in the $R = 6$ data sets. Upon closer examination, in the data sets with only 6 conditions Poisson mash RUV had much more difficulty distinguishing condition-specific expression differences β_{jr} from random effects η_{jr} ; in particular, Poisson mash RUV tended to attribute observed variability across conditions to random effects. To verify that this was indeed the case, we re-ran Poisson mash RUV without the random effects. This resulted in much better performance in all tasks (Figure 4). Recall, Poisson mash is applied to the condition-level aggregated data, so β_{jr} and η_{jr} are only identifiable by having priors with different cross-condition covariance structures (Section 5.1). In other words, Poisson mash relies solely on the patterns of observed variability across conditions to separate the two types

of effects, and is therefore expected to work better when we have data from more conditions.

While removing the random effect term was able to rescue the performance of Poisson mash RUV for $R = 6$ in this particular simulation, more generally it could hurt performance since random effects might exist and need to be accounted for. A better solution to this problem would be to collect multiple replicates within each condition, and to extend Poisson mash to allow for replicates; this should allow reliable estimation of the random effects by using the variability between the replicates in each condition (Appendix C). In the absence of this, users should be aware of the difficulty of distinguishing treatment vs. random effects (β_{jr} vs. η_{jr}) when analyzing data with few conditions (say, $R < 10$), and interpret results from Poisson mash or Poisson mash RUV with this in mind.

6.6 Bulk RNA-seq simulations with multiple replicates

While the focus of this paper is single-cell data, Poisson mash can also be applied to bulk data, in which the columns of \mathbf{Y} represent samples or replicates rather than cells. Therefore, we also evaluated Poisson mash in simulated bulk RNA-seq data sets. We simulated bulk RNA-seq data for $R = 12$ and $R = 25$ conditions, with 4 replicates per condition (for details see Appendix F.2). Then we applied Poisson mash to the data matrix \mathbf{X} obtained by summing RNA-seq counts across replicates from the same condition. We compared Poisson mash with mash and with two other methods (limma, edgeR) that are widely used to analyze bulk RNA-seq data. (Note that mash, edgeR and limma were applied to the sample-level data \mathbf{Y} , whereas Poisson mash was applied to the aggregated condition-level data \mathbf{X} . The methods were run on the bulk data sets in the same way as in the single-cell simulations.)

The results of these comparisons are shown in Supplementary Figure S3. Similar to the results on simulated single-cell data sets, Poisson mash provided considerable gains in detecting differential expression and in LFC estimation compared to limma and edgeR, which analyze the data from each condition independently. (Note that we did not include Poisson mash RUV in this experiment because we did not simulate these data with an “unwanted variation” component.) However, in contrast to the scRNA-seq simulations, mash and Poisson mash performed similarly well in all inference tasks; only in estimating the LFCs was Poisson mash marginally more accurate than mash across all simulation settings and gene expression levels (Supplementary Figure S3, Panels C and F). These results suggest that the bias in LFC estimates introduced by log-transformation is much less severe for bulk data; consider that the counts are much larger and less sparse in bulk data. Based on these results, we concluded that Poisson mash does not provide a clear advantage over mash for bulk RNA-seq data. Considering that mash is simpler and more flexible than Poisson mash — for example, mash can easily incorporate replicates, whereas this feature is not yet implemented in Poisson mash — our general recommendation would be to use mash for multi-condition, multi-replicate bulk RNA-seq data.

7 Application to cytokine stimulation data

To illustrate the potential for our methods to provide new insights in real applications, we analyzed data from a study of the effects of cytokine stimulation on gene expression. Single-cell RNA-seq data were collected from peripheral blood mononuclear cells (PBMCs) in cytokine-injected mice. Experiment protocols and data preparation steps are described in Appendix G. These data

were deposited into the Gene Expression Omnibus (GEO) data repository under accession number GSE214633.

The prepared data set contained UMI counts for 14,853 genes from 141,962 cells in $R = 45$ conditions (44 cytokine treatments and one control). Most of the cells (138,142) were assigned to one of 8 cell types based on expression of known marker genes (Supplementary Table S1 and Supplementary Data). Cells collected in each cytokine treatment condition were derived from three mice, but the information regarding which cells came from which mouse was not available. Therefore, DE analyses were performed as if there were just one replicate per condition.

To study changes in gene expression induced by cytokine stimulation, we applied Poisson mash RUV separately to the data for each of the 8 cell types. To account for unwanted variation, we estimated a $J \times D$ matrix \mathbf{F} , with $D = 4$, from the cell-level data \mathbf{Y} (see Appendix F.1.6).

For the mash prior, we included “canonical” covariance matrices capturing condition-specific expression differences, a “null” canonical covariance matrix for no effect in all conditions, and 7 data-driven covariance matrices. We estimated the data-driven covariance matrices separately in each cell type since the predominant sharing patterns might vary across cell types. In total, each mash prior was a mixture of $K = 45 + 1 + 7 = 53$ covariance matrices. After fitting the Poisson mash RUV model with a mash prior, we computed LFC estimates relative to the *median* across all conditions, which served as a more robust estimate of the baseline gene expression than the single control condition that could exhibit higher or lower gene expressions by chance.

Note that all of our analyses of these data used the Poisson mash RUV model, but for brevity we sometimes refer to the method as “Poisson mash”.

7.1 Poisson mash results for neutrophils

We begin with a more detailed investigation of the Poisson mash results for a single cell type — neutrophils — before summarizing the results for all 8 cell types. The prepared neutrophils data set contained expression data for 8,543 genes in 13,362 cells; among the 45 treatment conditions, the IL-1 α treatment had the most single-cell expression measurements (1,892 cells), and IL-13 had the fewest (41 cells) (Supplementary Table S1 and Supplementary Data). Based on the *minimum lfsr* with a threshold of $\alpha = 0.05$, Poisson mash identified 2,535 genes as being differentially expressed in at least one of the 45 conditions. In the presentation of the results, we focussed on a subset of 27 of the 45 conditions, omitting the control condition and the 17 chemokine treatments (chemokines are a distinctive subset of the cytokines) because these treatments tended to show much less differential expression and therefore the patterns of differential expression were much less interesting to look at.

Poisson mash assigned most of the weight (91%) in the mash prior to a single covariance matrix (Figure 5A). This covariance matrix captures particularly strong sharing of expression differences within two subsets of cytokines: (1) IL-1 α , IL-1 β , G-CSF; and (2) IL-12 p70, IFN- γ , IL-18, IL-15, IL-33. There are potential biological explanations for this structure. In the first subset, IL-1 α , IL-1 β stimulate the same receptor, IL-1R1 (Dinarello et al., 2012), and IL-1 has been shown to induce G-CSF production (Altmeier et al., 2016). We discuss this second subset below in our analyses across cell types. To verify these sharing patterns, we performed a factor analysis (Wang and Stephens, 2021) on the $2,535 \times 27$ matrix of posterior mean LFCs. This factor analysis yields both a set of *factors*, each of which captures a pattern of sharing of DE effects among cytokines, and a corresponding set of *loadings*, which quantify how strongly each gene exhibits each pattern. The top two factors in this factor analysis (Figure 5B) — when ranked by proportion of variance

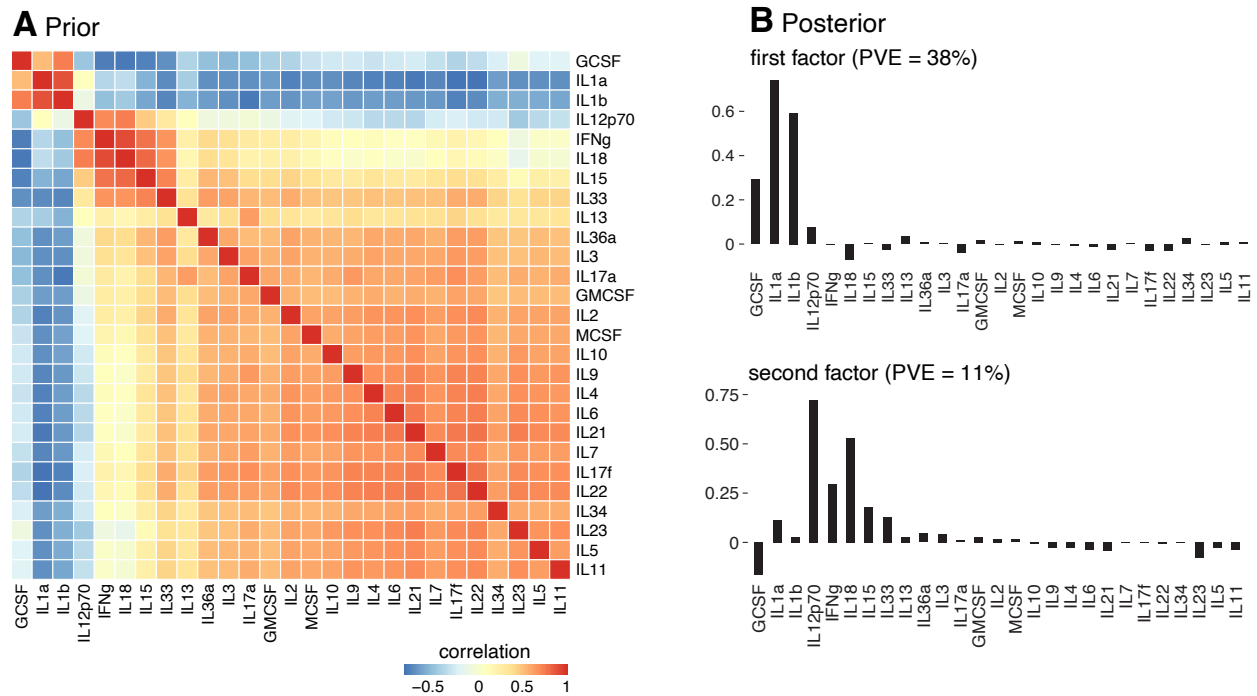


Figure 5: Patterns of differential expression across cytokine treatment conditions in the neutrophil data. The results shown here are for 27 of the 45 treatment conditions, omitting the control condition and the 17 chemokine treatments. Panel A shows correlations among cytokine treatments calculated from the top covariance matrix in the Poisson mash prior. The top covariance matrix is a data-driven covariance matrix, and accounts for 91% of the total weight of the prior. Panel B shows the top two factors by PVE (proportion of variance explained) from a factor analysis of the Poisson mash RUV posterior mean LFC estimates.

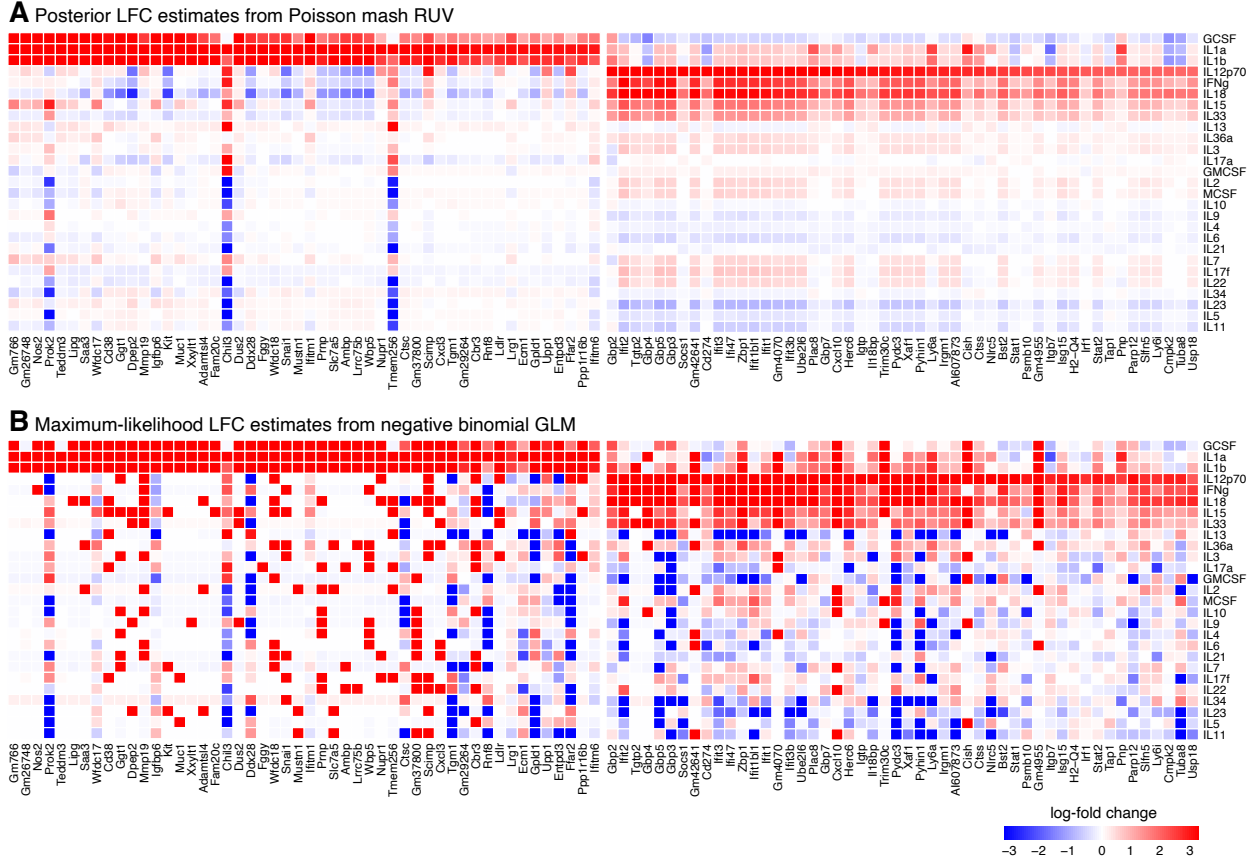


Figure 6: Multi-condition differential expression in neutrophils for selected genes as estimated by Poisson mash RUV (A) and a negative binomial GLM (B). The log-fold changes (in base-2 logarithm) are defined relative to the median expression level across cytokine treatments. Posterior mean estimates from Poisson mash RUV are shown in A, and maximum likelihood estimates from a negative binomial GLM model, fit separately to each gene, are shown in B. The selected genes are the 50 genes with the largest positive loadings in the first factor (Figure 5B), and another 50 genes with the largest positive loadings in the second factor (Figure 5B). Results are shown for 27 of the 45 conditions.

explained — capture similar patterns to those observed in the prior.

To highlight the value of having Poisson mash learn these patterns and then use these patterns to inform the estimation of DE effects, we compared the Poisson mash posterior mean LFC estimates to the maximum likelihood LFC estimates from a negative binomial (NB) GLM fit to the UMI counts, separately for each gene (Figure 6; we used the `glm.nb` function from the MASS R package). Reassuringly, the main patterns of shared DE effects are visually apparent in the maximum likelihood estimates, suggesting that our procedure is correctly identifying patterns that are present in the raw data. However, the maximum likelihood estimates can be noisy, especially for gene-condition pairs with small counts, and the stabilizing effect of the EB shrinkage estimation from Poisson mash is also visually apparent: the shrinkage estimation tends to “denoise” the LFC estimates by shrinking the smaller effects towards zero, and more generally making the estimates more concordant with the main patterns identified in the prior. Note that the effect estimates for the stronger effects are generally similar to the maximum likelihood estimates, illustrating that Poisson mash can regularize effect sizes adaptively and avoid over-shrinkage of true large effects.

For comparison, we also applied *mash* to these same data. (Specifically, we applied *mash* to the LFC statistics returned by running *limma* on the log-transformed UMI counts, as we did in the simulations.) Consistent with the results of the simulations, *mash* consistently produced posterior mean LFC estimates that were much smaller in magnitude than Poisson *mash* (results not shown).

Finally, we assessed the goodness-of-fit of the Poisson *mash* model fitted to the neutrophils data. The result of the goodness-of-fit analysis is a set of 8,543 p -values, one for each gene, from a test of whether the data for that gene could have been generated from the fitted model. The histogram of the 8,543 p -values does not show a strong excess of zero or extremely small p -values (Supplementary Figure S11). Although the data do not conform exactly to the Poisson *mash* model (the histogram is not uniform), there are no strong “outlier” genes that show very significant deviations from the fitted model.

7.2 Patterns of cytokine response in eight cell types

To investigate patterns of cytokine response in all eight cell types, we applied the procedure outlined above for neutrophils — Poisson *mash*, followed by a factor analysis of the Poisson *mash* posterior mean LFC estimates — separately to each of the eight cell types (Supplementary Table S1). To interpret the factors, we used the WebGestalt tool (Liao et al., 2019) to identify Gene Ontology (GO) gene sets (The Gene Ontology Consortium, 2020) that were enriched in “driving genes” for each factor, which refer to the genes that exhibit the most significant loadings ($lfsr < 0.001$) in that factor, then we grouped factors together that shared enriched GO gene sets. As above, these downstream analyses of the Poisson *mash* results were focussed on the 27 conditions with the strongest overall differential expression (omitting the control condition and the 17 chemokine treatments). See Supplementary Figures S4–S10 summarizing the results of the factor analyses, and see Supplementary Table S2 for details on the GO enrichment analyses.

Some of the factors captured patterns of cytokine response that were relatively consistent across cell types, both in terms of the types of cytokines involved and the enriched GO gene sets. These shared factors are listed in Supplementary Table S2. For example, the cytokines IL-12 p70, IL-18, IFN- γ , IL-15 and IL-33 — the second subset we mentioned earlier (Section 7.1) — were identified in a factor in most cell types (except for dendritic cells and NK cells, where such a factor could still exist but may be undetected due to insufficient number of cells). The driving genes for these factors were enriched for immune-related GO terms such as response to interferon-beta, response to interferon-gamma, and antigen processing and presentation. Consistent with this observation, previous studies have shown that these cytokines induce the production of interferons (Wojno et al., 2019; Jabri and Abadie, 2015; Dinarello, 2018) which are responsible for the regulation and activation of the immune system. For example, it has been shown that IL-18, initially named as “IFN- γ inducing factor”, can induce the production of IFN- γ by Th1 cells (Okamura et al., 1995). Furthermore, IL-12 p40 deficient mice, which lack both IL-12 p40 and IL-12 p70, are unable to control bacterial growth due to the absence of IFN- γ production from splenocyte (Cooper et al., 1997). In addition, combination of IL-12 and IL-18 induce IFN- γ production from B cells in vitro (Yoshimoto et al., 1997).

Other factors were more cell-type-specific, or at least more important to one cell type. These cell-type-specific factors are listed in Supplementary Table S3. For example, a factor capturing concordant response to cytokines IL-15, IFN- γ , IL-23, IL-17A, IL-17F, G-CSF, M-CSF appeared in CD4⁺ T cells only. The driving genes were enriched for GO terms such as response to wounding and fatty acid metabolic process. Studies have shown that IL-23 is required for full differentiation

of effector Th17 cells (McGeachy et al., 2009) which play a key role in tissue repair (Littman and Rudensky, 2010), and activation of mTOR signaling pathway (Chang et al., 2013) which is involved in regulation of lipid metabolism (Shimobayashi and Hall, 2014). In addition, previous studies have shown that IFN- γ induces the expansion of IL-17-producing CD4⁺ T cells during mycobacterial infection (Cruz et al., 2006), and intrathecal M-CSF expands CD4⁺ regulatory T cells (Kuhn et al., 2021), both of which are actively involved in wound healing and tissue repair (Boothby et al., 2020).

We also identified factors in different cell types enriched for GO terms related to cell cycle. This included factors capturing concordant changes in IL-33 and IL-4 in CD4⁺ T cells; IL-12 p70, IL-17A, IL-17F, IL-1 α , IL-4, IL-11, IL-15, IL-33 in CD8⁺ T cells; and IL-17A, IL-15, IL-1 β , IL-33, IL-34, IL-36 α in NK cells. Biologically, cell cycle is closely connected to cellular proliferation, so these results are consistent with the fact that different cytokines have been observed to induce proliferation in different cell types. Furthermore, these results are consistent with previous reports that IL-4, IL-33 and IL-15, respectively, induce the proliferation of CD4⁺ T cells, CD8⁺ T cells and NK cells (Zhu et al., 2002; Dreis et al., 2019; Jabri and Abadie, 2015).

8 Discussion

In this paper, we have introduced a flexible empirical Bayes method, “Poisson mash”, for analyzing count data from many features (e.g., genes) observed in multiple conditions (e.g., treatments). It estimates differences in the underlying mean parameters while accounting for different patterns of effects across conditions. Our methods extend the mash framework (Urbut et al., 2019) to analysis of Poisson data. Our work was motivated by differential expression analysis of multi-condition scRNA-seq data, but the model is not specific to scRNA-seq data and could also be useful for multivariate count data in other settings.

Although differential expression analysis of scRNA-seq data has been extensively studied, to the best of our knowledge our work is the first that allows for arbitrary patterns of correlation across multiple conditions, and uses these patterns to inform estimation and testing of multi-condition differential expression. Our approach can account for overdispersion of count data and unwanted variation. Compared to existing methods, our approach achieves substantial improvement in identifying and estimating expression differences. Another advantage of our empirical Bayes approach is that it yields posterior distributions for the effects, which can be used to estimate LFCs with respect to an arbitrary reference point such as the median across conditions. The posterior distributions can also be used to calculate the probability that an expression difference is larger than δ , where $\delta > 0$ is some chosen LFC threshold. For example, δ might be an LFC considered to be “biologically meaningful” (Bochkina and Richardson, 2007; McCarthy and Smyth, 2009). This probability can be computed by Monte Carlo simulation.

To fit the Poisson mash model, we used variational approximation techniques to obtain tractable and scalable computations. This approach involves approximating the true posterior of β_j , which does not have a closed form, by a mixture of multivariate Gaussians. We made no other approximations. In particular, we did not use a “mean field” approximation that makes conditional independence assumptions. Such conditional independence assumptions often do not hold in practice, and the mean field approximations are known to generally underestimate uncertainty in posterior distributions (Blei et al., 2017). The approximate posteriors in Poisson mash are expected to be accurate so long as a mixture of Gaussians is a good fit for the true posterior.

A well-calibrated *lfsr* provides a condition-specific measure of significance for DE testing. Our

simulations showed that when true the LFCs were sparse among conditions (i.e., non-null genes are differentially expressed in only a small subset of conditions, corresponding to sparse covariance matrices \mathbf{U}_k), the *lfsr* was underestimated by both mash and Poisson mash RUV. We found that this was mostly due to the use of data-driven rank-1 covariance matrices in the mash prior (Urbut et al., 2019). Rank-1 covariance matrices reduce computational cost and are often more interpretable, but they are also restrictive in that effects across conditions are forced to lie within a rank-1 subspace of \mathbb{R}^R and, as a result, this produces a *lfsr* that cannot vary among conditions. This issue could be partially addressed by adding a small positive number ϵ to the diagonals of prior covariance matrices \mathbf{U}_k . We found that choosing $\epsilon = 0.01$ worked well in multiple settings, and perhaps a better choice of ϵ could be chosen automatically from data. We reserve this question for future work. In addition, mis-estimation of the covariance matrices \mathbf{U}_k could also lead to *lfsr* calibration issues, and in particular estimating non-sparse \mathbf{U}_k when the true \mathbf{U}_k is sparse. Therefore, incorporating regularization in the estimation of \mathbf{U}_k to encourage sparsity could improve calibration of *lfsr*, and is a potential area of further investigation.

We took a “pseudobulk” approach that aggregates cells by condition before performing the DE analysis. This aggregation step inevitably leads to a loss of information, preventing us from capturing more complex patterns of DE between conditions (Zhang et al., 2022). One could consider instead modeling the cell-level counts. However, some previous studies (Lun and Marioni, 2017; Squair et al., 2021) have found that DE methods that aggregate cells from each replicate perform better than methods that model cell-level data and do not specifically account for inter-replicate variation or intra-replicate dependence. Therefore, it is not clear that the potential benefits of modeling cell-level counts would be worth the added complexity of modeling and computation.

Another limitation of our current implementation is that it assumes one replicate per condition. Incorporation of condition-specific random effects, $\boldsymbol{\eta}_j$, into our model softens this limitation, essentially by using variability across conditions to serve as an imperfect replacement for within-condition replicates. However, when multiple replicates are available in each condition, it would clearly be advantageous to use them, and this could improve the performance of Poisson mash when the number of conditions is small. Our model could be extended to this case (see Appendix C) but we have not yet implemented this and we leave it to future work.

Although Poisson mash was motivated by multi-condition data, in principle it should be straightforward to use Poisson mash to explore patterns of differential expression across multiple cell types. Since we have not applied Poisson mash for this purpose, it remains to be seen whether modeling shared effects is helpful for analyzing differences in expression across multiple cell types, but it seems plausible. One statistical issue that arises in such analyses is the “double-dipping” problem (Gao et al., 2022) which comes from performing differential expression analysis between groups that were, themselves, estimated from the same expression data. This double-dipping issue, however, is not specific to Poisson mash.

Acknowledgments

We thank Abhishek Sarkar, Yuxin Zou and Jason Willwerscheid for their invaluable advice. We also thank the staff at the Research Computing Center for providing the high-performance computing resources used to implement the numerical experiments.

Appendix A Modeling unwanted variation at the condition level vs. at the cell level

Here we justify applying the Poisson mash RUV model ((5.3) in the main text) to aggregated data \mathbf{X} when \mathbf{F} is estimated from cell-level data \mathbf{Y} . See the main text for definitions.

Consider the following model of the single-cell UMI counts,

$$\begin{aligned} y_{ji} &\sim \text{Pois}(\tilde{s}_i \tilde{\lambda}_{ji}) \\ \log \tilde{\lambda}_{ji} &= \mu_j + \sum_{r=1}^R \beta_{jr} \delta_{ri} + \sum_{d=1}^D f_{jd} \alpha_{di}, \end{aligned} \quad (\text{A.1})$$

in which $\delta_{ri} = 1$ if cell i is in condition r , otherwise $\delta_{ri} = 0$, and α_{di} denotes the d th unobserved factor causing unwanted variation in cell i . If we define the cell-level size factors, \tilde{s}_i , by the total UMI counts,

$$\tilde{s}_i = \sum_{j=1}^J y_{ji}$$

then it follows straightforwardly that the condition-level size factors can be expressed as sums of the cell-level size factors:

$$s_r := \sum_{j=1}^J x_{jr} = \sum_{i \in \mathcal{S}_r} \tilde{s}_i.$$

From this identity, the expected value of the aggregated count x_{jr} under model (A.1) is

$$\begin{aligned} \mathbb{E}[x_{jr}] &= \sum_{i \in \mathcal{S}_r} \mathbb{E}[y_{ji}] \\ &= \sum_{i \in \mathcal{S}_r} \tilde{s}_i \times \exp(\mu_j + \beta_{jr} + \sum_{d=1}^D f_{jd} \alpha_{di}) \\ &= \exp(\mu_j + \beta_{jr}) \times \sum_{i \in \mathcal{S}_r} \tilde{s}_i \exp(\sum_{d=1}^D f_{jd} \alpha_{di}). \end{aligned} \quad (\text{A.2})$$

Next, by a Taylor series expansion, we have

$$\begin{aligned} \mathbb{E}[x_{jr}] &\approx \exp(\mu_j + \beta_{jr}) \times \sum_{i \in \mathcal{S}_r} \tilde{s}_i (1 + \sum_{d=1}^D f_{jd} \alpha_{di}) \\ &= \exp(\mu_j + \beta_{jr}) \times \left\{ \sum_{i \in \mathcal{S}_r} \tilde{s}_i + \sum_{d=1}^D \sum_{i \in \mathcal{S}_r} \tilde{s}_i \alpha_{di} f_{jd} \right\} \\ &= s_r \times \exp(\mu_j + \beta_{jr}) \times \left\{ 1 + \sum_{d=1}^D f_{jd} \rho_{rd} \right\}, \end{aligned} \quad (\text{A.3})$$

in which define $\rho_{rd} := \sum_{i \in \mathcal{S}_r} \tilde{s}_i \alpha_{di} / s_r$. Finally, by a second Taylor series expansion, we have

$$\mathbb{E}[x_{jr}] \approx s_r \times \exp \left\{ \mu_j + \beta_{jr} + \sum_{d=1}^D f_{jd} \rho_{rd} \right\}. \quad (\text{A.4})$$

This result suggests that we can include the additional term $\sum_{d=1}^D f_{jd} \rho_{rd}$ in the Poisson mash model

to approximate the effect of the confounding variables on the aggregated counts \mathbf{X} .

Appendix B Extension to multiple subgroups

So far, we have assumed a baseline expression level, μ_j , that is shared across all conditions. We have also implemented the setting in which the R conditions are subdivided into M subgroups, and each subgroup $\mathcal{T}_m \subseteq \{1, \dots, R\}$, $m \in \{1, \dots, M\}$ has its own baseline μ_{jm} . For example, one may want to perform a multi-condition DE analysis in M cell types. The benefit of performing this analysis jointly for multiple conditions and multiple cell types is that we can leverage the sharing of expression differences across both conditions and cell types. The Poisson mash model for multiple subgroups is

$$\begin{aligned} x_{jr} &\sim \text{Pois}(s_r \lambda_{jr}), \\ \log \lambda_{jr} &= \mu_{jm(r)} + \beta_{jr} \\ \beta_j &\sim \sum_{k=1}^K \sum_{l=1}^L \pi_{kl} N_R(\mathbf{0}, w_l \mathbf{U}_k), \end{aligned} \tag{B.1}$$

in which $m(r)$ denotes the mapping from indices $r \in \{1, \dots, R\}$ to subgroups $m \in \{1, \dots, M\}$ that corresponds to the partitioning $\{\mathcal{T}_1, \dots, \mathcal{T}_M\}$.

Appendix C Extension to multiple replicates per condition (not implemented)

In the paper, we assumed only one replicate per condition. Here we briefly describe the extension of Poisson mash to handle multiple replicates per condition. This has the potential to improve estimation of inter-replicate variances ψ_j^2 and therefore can help to address identifiability issues (see Section 5.1 of the main text). *Please note that we have not yet implemented this extension, and we only describe this extension here to illustrate the potential of Poisson mash to be applied to data sets with multiple replicates.*

Instead of aggregating the counts by condition, we aggregate the counts by replicate; that is, x_{jt} is the aggregated count for gene j , replicate t , and s_t is the size factor for replicate t .

The Poisson mash RUV model for data with replicates is

$$\begin{aligned} x_{jt} &\sim \text{Pois}(s_t \lambda_{jt}) \\ \log \lambda_{jt} &= \mu_j + \beta_{jr} + \eta_{jt} + \sum_{d=1}^D f_{jd} \rho_{td}, \quad t \in \mathcal{T}_r. \end{aligned} \tag{C.1}$$

As before, β_j is a vector of length R , and is assigned the mash prior (3.1); the random effects vector η_j is a vector of length $N_T := \sum_{r=1}^R |\mathcal{T}_r|$ in which the individual elements are drawn independently from the normal distribution with mean zero and variance ψ_j^2 . Also note that the matrix of unobserved factors, ρ , is a $N_T \times D$ matrix.

Appendix D Goodness-of-fit test

Here we describe the test to assess goodness-of-fit for a Poisson mash model. The description we give here is for the basic Poisson mash model, but the same ideas easily extend to the Poisson mash

models with the various enhancements.

First, for gene j , we define the “best ELBO”, denoted by ELBO_j^* , as the best lower bound that can be attained for a given setting of the model parameters:

$$\text{ELBO}_j^*(\mu_j, \boldsymbol{\pi}, \mathbf{U}, \mathbf{x}_j) := \max_{q_j} \text{ELBO}_j(q_j; \mu_j, \boldsymbol{\pi}, \mathbf{U}, \mathbf{x}_j). \quad (\text{D.1})$$

Note we have modified the notation slightly here to make explicit the dependence on the data, \mathbf{x}_j . This quantity is lower bound to the log-likelihood, $\log p(\mathbf{x}_j \mid \mu_j, \boldsymbol{\pi}, \mathbf{U})$, and can be interpreted as an approximate goodness-of-fit measure for data \mathbf{x}_j .

The goodness-of-fit test proceeds as follows. For gene j , we draw i.i.d samples $\mathbf{x}_j^{(i)}$, $i = 1, \dots, n_s$, from the fitted Poisson mash model, where n_s is a (typically large) number of Monte Carlo samples. Then we compute

$$\frac{1}{n_s} \sum_{i=1}^{n_s} \mathbb{1}\{\text{ELBO}_j^*(\mu_j, \boldsymbol{\pi}, \mathbf{U}, \mathbf{x}_j) > \text{ELBO}_j^*(\mu_j, \boldsymbol{\pi}, \mathbf{U}, \mathbf{x}_j^{(i)})\}. \quad (\text{D.2})$$

This quantity can be used like a p -value: if it is zero or close to zero, it suggests that the Poisson mash model provides a poor fit for \mathbf{x}_j ; if the Poisson mash model fits the data well, the p -values across genes j should roughly be uniformly distributed over the $[0, 1]$ interval.

Appendix E Model fitting algorithms

We now derive algorithms for fitting the Poisson mash RUV model to data with multiple subgroups. For convenience, we summarize the model here:

$$\begin{aligned} x_{jr} &\sim \text{Pois}(s_r \lambda_{jr}), \\ \log \lambda_{jr} &= \mu_{jm(r)} + \beta_{jr} + \eta_{jr} + \sum_{d=1}^D f_{jd} \rho_{rd} \\ \boldsymbol{\beta}_j &\sim \sum_{k=1}^K \sum_{l=1}^L \pi_{kl} N_R(\mathbf{0}, w_l \mathbf{U}_k) \\ \boldsymbol{\eta}_j &\sim N_R(\mathbf{0}, \psi_j^2 \mathbf{I}_R). \end{aligned} \quad (\text{E.1})$$

The other variants of the Poisson mash model are special cases of this model, and therefore the algorithms for Poisson mash RUV with multiple subgroups can also be applied to the other variants of Poisson mash.

E.1 Gaussian variational approximation

In the main text, we described the posterior distribution for $\boldsymbol{\beta}_j$, and its Gaussian approximation, in the basic Poisson mash model. Here we need to generalize the approach to the Poisson mash RUV model. To derive the more general approach, we define $\boldsymbol{\theta}_j := \boldsymbol{\beta}_j + \boldsymbol{\eta}_j$, and we consider the posterior distribution of $\boldsymbol{\theta}_j$, which is

$$p_{\text{post}}(\boldsymbol{\theta} \mid \mathbf{x}_j, \boldsymbol{\Omega}) \propto p(\mathbf{x}_j \mid \boldsymbol{\theta}_j, \boldsymbol{\Omega}) \times \sum_{k=1}^K \sum_{l=1}^L \pi_{kl} N_R(\boldsymbol{\theta}_j; \mathbf{0}, w_l \mathbf{U}_k + \psi_j^2 \mathbf{I}_R), \quad (\text{E.2})$$

where $\boldsymbol{\Omega} := \{\boldsymbol{\mu}, \boldsymbol{\pi}, \mathbf{U}, \psi^2, \boldsymbol{\rho}\}$ denote the parameters to be estimated for the Poisson mash RUV model.

Since this posterior does not have a closed form, we approximate it by a mixture of multivariate normals,

$$q_j(\boldsymbol{\theta}_j) = \sum_{k=1}^K \sum_{l=1}^L \zeta_{jkl} N_R(\boldsymbol{\theta}_j; \boldsymbol{\varphi}_{jkl}, \boldsymbol{\Sigma}_{jkl}). \quad (\text{E.3})$$

Or, introducing the latent indicator variable \mathbf{z}_j as we did in the main text, the approximate posterior is

$$q_j(\boldsymbol{\theta}_j, \mathbf{z}_j) = \prod_{k=1}^K \prod_{l=1}^L \{\zeta_{jkl} N_R(\boldsymbol{\theta}_j; \boldsymbol{\varphi}_{jkl}, \boldsymbol{\Sigma}_{jkl})\}^{z_{jkl}}. \quad (\text{E.4})$$

E.2 Evidence lower bound (ELBO)

We estimate the model parameters $\boldsymbol{\Omega}$ and the approximate posteriors q_1, \dots, q_J by maximizing the ELBO:

$$\text{ELBO}(q; \boldsymbol{\Omega}) = \sum_{j=1}^J \text{ELBO}_j(q_j; \boldsymbol{\Omega}), \quad (\text{E.5})$$

in which the ELBO for gene j is

$$\text{ELBO}_j(q_j; \boldsymbol{\Omega}) = \log p(\mathbf{x}_j \mid \boldsymbol{\mu}_j, \boldsymbol{\Omega}) - D_{\text{KL}}(q_j(\boldsymbol{\theta}_j, \mathbf{z}_j) \parallel p_{\text{post}}(\boldsymbol{\theta}_j, \mathbf{z}_j)) \quad (\text{E.6})$$

$$= \sum_{k=1}^K \sum_{l=1}^L \zeta_{jkl} \{ \log(\pi_{kl}/\zeta_{jkl}) + \Psi_{jkl}(\boldsymbol{\varphi}_{jkl}, \boldsymbol{\Sigma}_{jkl}; \boldsymbol{\Omega}) \}, \quad (\text{E.7})$$

where

$$\begin{aligned} \Psi_{jkl}(\boldsymbol{\varphi}_{jkl}, \boldsymbol{\Sigma}_{jkl}; \boldsymbol{\Omega}) &:= \mathbb{E}_q[\log p(\mathbf{x}_j \mid \boldsymbol{\theta}_j, \boldsymbol{\Omega})] \\ &\quad - D_{\text{KL}}(N_R(\boldsymbol{\theta}_j; \boldsymbol{\varphi}_{jkl}, \boldsymbol{\Sigma}_{jkl}) \parallel N_R(\boldsymbol{\theta}_j; \mathbf{0}, w_l \mathbf{U}_k + \psi_j^2 \mathbf{I}_R)). \end{aligned} \quad (\text{E.8})$$

Expanding terms, this is

$$\begin{aligned} \Psi_{jkl}(\boldsymbol{\varphi}_{jkl}, \boldsymbol{\Sigma}_{jkl}; \boldsymbol{\Omega}) &= \sum_{r=1}^R \left\{ x_{jr} \left(\log s_r + \mu_{jm(r)} + \varphi_{jklr} + \sum_{d=1}^D f_{jd} \rho_{rd} \right) \right. \\ &\quad \left. - s_r \exp \left(\mu_{jm(r)} + \varphi_{jklr} + \frac{1}{2} \sigma_{jkl,rr} + \sum_{d=1}^D f_{jd} \rho_{rd} \right) \right. \\ &\quad \left. - \log(x_{jr}!) \right\} \\ &\quad - D_{\text{KL}}(N_R(\boldsymbol{\theta}_j; \boldsymbol{\varphi}_{jkl}, \boldsymbol{\Sigma}_{jkl}) \parallel N_R(\boldsymbol{\theta}_j; \mathbf{0}, w_l \mathbf{U}_k + \psi_j^2 \mathbf{I}_R)). \end{aligned}$$

Algorithm 1 Variational Bayes for Poisson mash RUV with fixed prior covariances.

Require: Count data \mathbf{X} ($J \times R$ matrix), size factors \mathbf{s} (vector of length R), and additional covariates \mathbf{F} capturing unwanted variation ($J \times D$ matrix).

Require: Prior covariances $\mathbf{U}_1, \dots, \mathbf{U}_K$ ($R \times R$ matrices) and prior scaling factors $w_1, \dots, w_L \geq 0$.

Require: Initial estimates of the model parameters, $\boldsymbol{\rho}, \boldsymbol{\pi}$.

Require: Initial estimates of the approximate posteriors, $\boldsymbol{\varphi}, \boldsymbol{\Sigma}, \boldsymbol{\zeta}$.

Require: Convergence tolerances $\epsilon_\mu, \epsilon_\psi, \epsilon_\Upsilon \geq 0$.

$\boldsymbol{\Upsilon} = \mathbf{F}\boldsymbol{\rho}'$

repeat

 Perform all updates (E.9) and store the result in $\boldsymbol{\mu}^{\text{new}}$.

 Perform all updates (E.10) and store the result in $(\boldsymbol{\psi}^2)^{\text{new}}$.

 Compute $\text{argmax}_\rho \text{ELBO}(q; \boldsymbol{\Omega})$ and store the result in $\boldsymbol{\rho}$ (see eq. E.12).

$\boldsymbol{\Upsilon}^{\text{new}} = \mathbf{F}\boldsymbol{\rho}'$

$\mathcal{J}_{\text{update}} \leftarrow \{j : |(\psi_j^2)^{\text{new}} - \psi_j^2| > \epsilon_\psi \text{ or } \max_m |\mu_{jm}^{\text{new}} - \mu_{jm}| > \epsilon_\mu \text{ or } \max_r |\Upsilon_{jr}^{\text{new}} - \Upsilon_{jr}| > \epsilon_\Upsilon\}$

for $j = 1, \dots, J$ **do**

if $j \in \mathcal{J}_{\text{update}}$ **then**

$\boldsymbol{\mu}_j \leftarrow \boldsymbol{\mu}_j^{\text{new}}$

$\psi_j^2 \leftarrow (\psi_j^2)^{\text{new}}$

$\boldsymbol{\Upsilon}_j \leftarrow \boldsymbol{\Upsilon}_j^{\text{new}}$

 For each k, l , compute $\text{argmax}_{\boldsymbol{\varphi}_{jkl}, \boldsymbol{\Sigma}_{jkl}} \text{ELBO}(q; \boldsymbol{\Omega})$ by iterating (E.14–E.16).

end if

end for

 Perform all updates (E.13) and store the result in $\boldsymbol{\zeta}$.

 Perform all updates (E.11) and store the result in $\boldsymbol{\pi}$.

until $\mathcal{I} = \emptyset$.

return parameter estimates $\boldsymbol{\mu}, \boldsymbol{\psi}^2, \boldsymbol{\rho}, \boldsymbol{\pi}$ and posterior estimates $\boldsymbol{\varphi}, \boldsymbol{\Sigma}, \boldsymbol{\zeta}$.

E.3 Model fitting algorithm with fixed prior covariance matrices

We now describe a *coordinate ascent algorithm* for fitting the Poisson mash RUV model with Gaussian variational approximations to the posterior distributions of the unknowns $\boldsymbol{\theta}_j$. For now, we assume that the prior covariances $\mathbf{U}_1, \dots, \mathbf{U}_K$ are known, and below we will describe an algorithm to estimate them.

The model fitting algorithm is summarized in Algorithm 1.

The most computationally intensive step in Algorithm 1 is the updating of the approximate posteriors for each gene j . To reduce computation without greatly impacting accuracy, we selectively update the posteriors based on the updates to the model parameters. The idea is that if the parameters for gene j did not change much, the posterior for gene j will most likely not change much either. The genes j to be updated are stored in $\mathcal{J}_{\text{update}}$.

E.3.1 Coordinate ascent updates for the model parameters

The update for the subgroup-specific baseline expression levels $\boldsymbol{\mu}$ maximizing the ELBO (E.5) with the other parameters kept fixed is

$$\begin{aligned} \mu_{jm}^{\text{new}} &= \log \left\{ \sum_{r \in \mathcal{T}_m} x_{jr} \right\} \\ &\quad - \log \left\{ \sum_{r \in \mathcal{T}_m} \sum_{k=1}^K \sum_{l=1}^L s_r \zeta_{jkl} \exp \left(\sum_{d=1}^D f_{jd} \rho_{rd} + \varphi_{jklr} + \frac{1}{2} \sigma_{jkl,rr} \right) \right\}. \end{aligned} \quad (\text{E.9})$$

The update for $\boldsymbol{\psi}^2$ maximizing the ELBO (E.5) with the other parameters unchanged is

$$\begin{aligned} (\psi_j^2)^{\text{new}} &= \frac{1}{R} \mathbb{E}_{q_j} [\boldsymbol{\eta}'_j \boldsymbol{\eta}_j] \\ &= \frac{1}{R} \sum_{k=1}^K \sum_{l=1}^L \zeta_{jkl} \mathbb{E}_{q_j} [\boldsymbol{\eta}'_j \boldsymbol{\eta}_j \mid z_{jkl} = 1]. \end{aligned} \quad (\text{E.10})$$

The expectations in this expression have a closed form because the approximate posterior conditioned on the indicator variables z_{jkl} is multivariate normal.

The update for the mixture weights $\boldsymbol{\pi}$ maximizing the ELBO (E.5) with the other parameters kept fixed is simply

$$\pi_{kl}^{\text{new}} = \frac{1}{J} \sum_{j=1}^J \zeta_{jkl}. \quad (\text{E.11})$$

The update for $\boldsymbol{\rho}$ does not have a closed form, so instead we found the maximizer by Newton's method. Because the ELBO (E.5) is separable over the R rows of $\boldsymbol{\rho}$, we can compute the maximizer separately for each row of $\boldsymbol{\rho}$:

$$\begin{aligned} \rho_{r1}^*, \dots, \rho_{rD}^* &:= \underset{\rho_{r1}, \dots, \rho_{rD}}{\operatorname{argmax}} \operatorname{ELBO}(q; \boldsymbol{\Omega}) \\ &= \underset{\rho_{r1}, \dots, \rho_{rD}}{\operatorname{argmax}} \left\{ \sum_{j=1}^J \sum_{d=1}^D x_{jr} f_{jd} \rho_{rd} \right. \\ &\quad \left. - \sum_{j=1}^J \sum_{k=1}^K \sum_{l=1}^L s_r \zeta_{jkl} \exp \left(\mu_{jm(r)} + \sum_{d=1}^D f_{jd} \rho_{rd} + \varphi_{jklr} + \frac{1}{2} \sigma_{jkl,rr} \right) \right\}. \end{aligned} \quad (\text{E.12})$$

E.3.2 Coordinate ascent updates for the approximate posteriors

The remaining part of the coordinate ascent algorithm are the updates for the approximate posteriors q_j .

The mixture weights $\boldsymbol{\zeta}$ maximizing the ELBO—subject to the constraints that they are non-negative and sum to 1 for each j —have the following closed-form solution:

$$\zeta_{jkl}^{\text{new}} \propto \pi_{kl} \exp \{ \Psi_{jkl}(\boldsymbol{\varphi}_{jkl}, \boldsymbol{\Sigma}_{jkl}; \boldsymbol{\Omega}) \}. \quad (\text{E.13})$$

The updates to the posterior means and covariances do not have closed-form solutions; instead we use the algorithm of Arridge et al. (2018). This algorithm involves iterating the following three updates until some convergence criterion is met or until some predetermined upper bound on the

number of iterations is reached:

$$a_{jklr} = s_r \exp \left\{ \mu_{jm(r)} + \sum_{d=1}^D \rho_{rd} f_{jd} + \varphi_{jklr} + \frac{1}{2} \sigma_{jkl,rr} \right\} \quad (\text{E.14})$$

$$\boldsymbol{\Sigma}_{jkl}^{\text{new}} = \left((w_l \mathbf{U}_k + \psi_j^2 \mathbf{I}_R)^{-1} + \text{diag}(\mathbf{a}_{jkl}) \right)^{-1} \quad (\text{E.15})$$

$$\boldsymbol{\varphi}_{jkl}^{\text{new}} = \boldsymbol{\varphi}_{jkl} - \boldsymbol{\Sigma}_{jkl}^{\text{new}} \left[\mathbf{a}_{jkl} - \mathbf{x}_j + \left(w_l \mathbf{U}_k + \psi_j^2 \mathbf{I}_R \right)^{-1} \boldsymbol{\varphi}_{jkl} \right], \quad (\text{E.16})$$

where $\mathbf{a}_{jkl} := (a_{jkl1}, \dots, a_{jklR})'$.

E.4 Model fitting algorithm with unknown prior covariance matrices

Here we describe estimation of the “data-driven” covariance matrices \mathbf{U}_k using a simplified Poisson mash RUV model. These estimated covariance matrices (possibly combined with other covariance matrices, such as “canonical” covariance matrices) are then used to fit the final Poisson mash RUV model (Algorithm 1).

To estimate the data-driven covariance matrices \mathbf{U}_k , we fit a slightly simplified Poisson mash RUV model (E.1) without the mixture over the different scales; specifically, with $L = 1$ and $\omega_1 = 1$. Since l is always 1, in the expressions we drop the “ l ” subscripts, and the mash prior for this simplified model is

$$\boldsymbol{\beta}_j \sim \sum_{k=1}^K \pi_k N_R(\mathbf{0}, \mathbf{U}_k). \quad (\text{E.17})$$

Similarly, without the mixture over the different scales, the approximate posterior is

$$q_j(\boldsymbol{\theta}_j, \mathbf{z}_j) = \prod_{k=1}^K \left\{ \zeta_{jk} N_R(\boldsymbol{\theta}_j; \boldsymbol{\varphi}_{jk}, \boldsymbol{\Sigma}_{jk}) \right\}^{z_{jk}}. \quad (\text{E.18})$$

Not using a mixture of scales in the mash prior is somewhat justified by the fact that we fit this model only to the genes with the strongest effects (see Section F.1.6).

As before, we take a coordinate ascent approach to optimizing the ELBO. Most of the coordinate ascent updates derived above can be reused here by setting $L = 1, w_l = 1$. The only update we still need to derive is the update for \mathbf{U}_k . Since some of these \mathbf{U}_k may be rank-1 matrices, we also derive special updates for rank-1 covariance matrices to take advantage of their special properties. The coordinate ascent algorithm is summarized in Algorithm 2.

E.4.1 Update for the full-rank prior covariance matrices

For the simplified Poisson mash RUV model (E.17), the ELBO, after dropping terms that do not involve \mathbf{U}_k , is

$$\begin{aligned} \text{ELBO}(q; \boldsymbol{\Omega}) &= \sum_{j=1}^J \zeta_{jk} \mathbb{E}_{q_j} \left[\log N_R(\boldsymbol{\beta}_j; \mathbf{0}, \mathbf{U}_k) \mid z_{jk} = 1 \right] + \text{constant} \\ &= -\frac{1}{2} \sum_{j=1}^J \zeta_{jk} \left\{ \log |\mathbf{U}_k| + \text{tr}(\mathbf{U}_k^{-1} \mathbb{E}_{q_j} [\boldsymbol{\beta}_j \boldsymbol{\beta}_j' \mid z_{jk} = 1]) \right\} + \text{constant}. \end{aligned} \quad (\text{E.19})$$

Algorithm 2 Variational Bayes for Poisson mash RUV with simplified model and unknown prior covariances.

Require: Count data \mathbf{X} ($J \times R$ matrix), size factors \mathbf{s} (vector of length R), and additional covariates \mathbf{F} capturing unwanted variation ($J \times D$ matrix).

Require: Initial estimates of the prior covariance matrices $\mathbf{U}_1, \dots, \mathbf{U}_K$. The rank-1 covariance matrices are represented by vectors \mathbf{u}_k such that $\mathbf{U}_k = \mathbf{u}_k \mathbf{u}_k'$.

Require: Initial estimates of the other model parameters, $\boldsymbol{\mu}, \psi^2, \boldsymbol{\rho}, \boldsymbol{\pi}$.

repeat

for $j = 1, \dots, J$ **do**

 For each k, l , compute $\operatorname{argmax}_{\boldsymbol{\varphi}_{jk}, \boldsymbol{\Sigma}_{jk}} \text{ELBO}(q; \boldsymbol{\Omega})$ by iterating (E.14–E.16).

 Update $\zeta_{j1}, \dots, \zeta_{jK}$ using (E.13).

end for

for $k = 1, \dots, K$ **do**

if \mathbf{U}_k is a rank-1 matrix **then**

 Perform update (E.24) and store the result in \mathbf{u}_k .

$\mathbf{U}_k \leftarrow \mathbf{u}_k \mathbf{u}_k'$

else

 Perform update (E.20) and store the result in \mathbf{U}_k .

end if

end for

 Perform all updates (E.9) and store the result in $\boldsymbol{\mu}$.

 Perform all updates (E.10) and store the result in ψ^2 .

 Compute $\operatorname{argmax}_{\boldsymbol{\rho}} \text{ELBO}(q; \boldsymbol{\Omega})$ and store the result in $\boldsymbol{\rho}$ (see eq. E.12).

 Perform all updates (E.11) and store the result in $\boldsymbol{\pi}$.

until convergence criterion is met

return $\mathbf{U}_1, \dots, \mathbf{U}_K$

Therefore, we have the following closed-form update for the full-rank covariance matrix \mathbf{U}_k :

$$\mathbf{U}_k^{\text{new}} = \frac{\sum_{j=1}^J \zeta_{jk} \mathbb{E}_{q_{jk}}[\boldsymbol{\beta}_j \boldsymbol{\beta}_j' \mid z_{jk} = 1]}{\sum_{j=1}^J \zeta_{jk}}. \quad (\text{E.20})$$

Using the fact that the distribution of $\boldsymbol{\beta}_j \mid z_{jk} = 1$ is multivariate normal under the variational approximation, the expectations (E.20) in work out to

$$\begin{aligned} \mathbb{E}_{q_j}[\boldsymbol{\beta}_j \boldsymbol{\beta}_j' \mid z_{jk} = 1] &= (\mathbf{U}_k^{-1} + \mathbf{I}_R / \psi_j^2)^{-1} \\ &\quad + (\psi_j^2 \mathbf{U}_k^{-1} + \mathbf{I}_R)^{-1} (\boldsymbol{\varphi}_{jk} \boldsymbol{\varphi}_{jk}' + \boldsymbol{\Sigma}_{jk}) (\psi_j^2 \mathbf{U}_k^{-1} + \mathbf{I}_R)^{-1}. \end{aligned} \quad (\text{E.21})$$

E.4.2 Update for the rank-1 prior covariance matrices

If \mathbf{U}_k is a rank-1 covariance matrix, the mash prior conditioned on $z_{jk} = 1$, $\boldsymbol{\beta}_j \mid z_{jk} = 1 \sim N_R(\mathbf{0}, \mathbf{U}_k)$, can be written as

$$\begin{aligned} \boldsymbol{\beta}_j &= v_j \mathbf{u}_k \\ v_j &\sim N(0, 1), \end{aligned} \quad (\text{E.22})$$

where $\mathbf{U}_k = \mathbf{u}_k \mathbf{u}'_k$. We can use this result to write an update expression that is equivalent to the update above, but has computational advantages; in particular, it avoids some expensive matrix operations on $R \times R$ matrices such as matrix inversions.

After dropping terms that do not depend on \mathbf{U}_k , the ELBO is

$$\begin{aligned} \text{ELBO}(q; \boldsymbol{\Omega}) &= \sum_{j=1}^J \zeta_{jk} \mathbb{E}_{q_j} [\log N(\boldsymbol{\theta}_j; v_j \mathbf{u}_k, \psi_j^2 \mathbf{I}_R) \mid z_{jk} = 1] + \text{constant} \\ &= \sum_{j=1}^J \frac{\zeta_{jk} \mathbf{u}'_k \mathbb{E}_{q_j} [v_j \boldsymbol{\theta}_j \mid z_{jk} = 1]}{\psi_j^2} - \sum_{j=1}^J \frac{\zeta_{jk} \mathbf{u}'_k \mathbf{u}_k \mathbb{E}_{q_j} [v_j^2 \mid z_{jk} = 1]}{2\psi_j^2} + \text{constant}. \end{aligned} \quad (\text{E.23})$$

Solving for \mathbf{u}_k yields the following update:

$$\mathbf{u}_k^{\text{new}} = \frac{\sum_{j=1}^J \zeta_{jk} / \psi_j^2 \times \mathbb{E}_{q_j} [v_j \boldsymbol{\theta}_j \mid z_{jk} = 1]}{\sum_{j=1}^J \zeta_{jk} / \psi_j^2 \times \mathbb{E}_{q_j} [v_j^2 \mid z_{jk} = 1]}, \quad (\text{E.24})$$

where

$$\mathbb{E}_{q_j} [v_j^2] = \frac{\psi_j^2 + \mathbf{u}'_k \mathbb{E}_{q_j} [v_j \boldsymbol{\theta}_j]}{\mathbf{u}'_k \mathbf{u}_k + \psi_j^2} \quad (\text{E.25})$$

$$\mathbb{E}_{q_j} [v_j \boldsymbol{\theta}_j] = (\boldsymbol{\varphi}_{jk} \boldsymbol{\varphi}'_{jk} + \boldsymbol{\Sigma}_{jk}) \times \frac{\mathbf{u}_k}{\mathbf{u}'_k \mathbf{u}_k + \psi_j^2}. \quad (\text{E.26})$$

Appendix F Other simulation details

Additional details about the simulations are given in this section.

F.1 Details of the methods compared in the simulations

Here we describe in detail how we ran each of the DE analysis methods in the simulations.

F.1.1 limma

We used the *limma-trend* method (Law et al., 2014; Phipson et al., 2016; Smyth, 2004) implemented in the *limma* R package (version 3.48.3; Ritchie et al. 2015). This involved the following steps. First, normalization factors were computed using the edgeR function `calcNormFactors` with the (default) “trimmed mean of M-values” method (Robinson and Oshlack, 2010). Then we computed log-normalized counts using the `cpm` function from edgeR with `log = TRUE` and `prior.count = 3`. Next, we fit a linear model to the log-normalized counts using the *limma* function `lmFit`, with conditions as variables; specifically, we chose the “design matrix” as `model.matrix(~0 + conditions)`, where `conditions` was a categorical variable encoding the assignment of cells to conditions. We reported maximum-likelihood estimates of the LFCs. For DE detection, we used the p -values from the moderated F -statistics which were obtained by the function `eBayes` with settings `trend = TRUE` and `robust = TRUE` (Law et al., 2014; Phipson et al., 2016). Note that, because the number of cells in each condition was quite large, the moderated F -statistics rarely differed

much from the unmoderated F -statistics. Still, the final p -values were based on the moderated F -statistics.

F.1.2 MAST

The MAST R package (version 1.18.0; [McDavid et al. 2021](#)) implements the hurdle GLM model proposed in [Finak et al. \(2015\)](#). Like `limma`, we fit the MAST model to the log-normalized counts in which conditions were included as variables in the GLM. The log-normalized counts were computed in the same way as in `limma`, except that we set `prior.count = 1`. As suggested by [Soneson and Robinson \(2018\)](#), we also included the cellular detection rate (the fraction of genes detected in each cell) as a covariate. We fit the GLM using the `zlm` function from MAST, keeping all default settings. For detecting DE genes, we used the p -values from the likelihood-ratio test (implemented by function `lrTest` in MAST). For detecting and estimating condition-level changes in expression, we called `getLogFC` to get LFC estimates and variances of these estimates. Two-tailed p -values were obtained from the z -scores, and these were used to identify differentially expressed gene-condition pairs.

F.1.3 Kruskal-Wallis test

We performed the Kruskal-Wallis rank-sum test ([Kruskal and Wallis, 1952](#)) on \mathbf{Y} using function `kruskal.test` from the `stats` R package, in which the conditions defined the groups for the Kruskal-Wallis test.

F.1.4 edgeR

We used the `edgeR` package (version 3.34.1; [McCarthy et al. 2012](#); [Robinson et al. 2010](#)) to fit a negative binomial GLM to the counts \mathbf{Y} , in which conditions were treated as variables in the GLM. Following [Soneson and Robinson \(2018\)](#), we included the cellular detection rate as an additional variable. We used `edgeR` functions `estimateDisp` followed by `glmQLFit` to fit the GLM, and tested DE effects by the quasi-likelihood-ratio test using `glmQLFTest` ([Chen et al., 2016](#); [Lun et al., 2016](#); [Lun and Smyth, 2017](#); [Lund et al., 2012](#)). Similar to `limma`, we set the design matrix to be `model.matrix(~0 + cdr + conditions)`, where `cdr` was the estimated cellular detection rate. Note that `edgeR` does not provide estimates of the standard error, and therefore cannot be used in combination with `mash`; see for example <https://support.bioconductor.org/p/61640>. We found that `edgeR` typically took much longer to run than `limma` or MAST.

F.1.5 mash

We used the `mashr` package (version 0.2.59; [Urbut et al. 2019](#)) to fit a multivariate adaptive shrinkage (“`mash`”) model to condition-level expression estimates produced by `limma`. Specifically, we applied a variant of `mash`, “common baseline `mash`”, which is intended for testing and estimating differences relative to a common reference point such as a control condition ([Urbut, 2017](#); [Zou, 2021](#)).

We took the following steps to fit the common baseline `mash` model and recover `mash` posterior quantities:

- (i) *Normalize and transform counts.* We computed log-normalized counts \tilde{y}_{ji} as

$$\tilde{y}_{ji} = \log(0.1 + y_{ji} \times \text{median}\{\tilde{s}_1, \dots, \tilde{s}_n\} / \tilde{s}_i),$$

in which $\tilde{s}_i := \sum_{j=1}^J y_{ji}$ is the size factor for cell i . This was guided by the discussion in Chapter 2 of [Willwerscheid \(2021\)](#).

- (ii) *Run limma.* We ran limma on the log-normalized counts \tilde{y}_{ji} as before (Section [F.1.1](#)), except that here we set `trend = TRUE`, `robust = FALSE`.
- (iii) *Define mash inputs.* The inputs to mash were the $J \times R$ matrix of condition-level expression estimates for all genes and the corresponding $J \times R$ matrix of standard errors. Since the conditions were randomly shuffled in the simulations, there was no correlations in the expression measurements among conditions, so we set \mathbf{C} to be the $R \times R$ identity matrix (which is the default setting in `mash_set_data`).
- (iv) *Define prior covariance matrices.* mash requires the covariance matrices \mathbf{U}_k in the prior to be specified beforehand. We defined a total of $K = R + 11$ prior covariance matrices, in which some were “canonical” covariance matrices, and others were “data-driven” matrices ([Urbut et al., 2019](#)).
- (a) *Define canonical covariance matrices.* First, we defined the $R + 5$ canonical covariance matrices \mathbf{U}_k by calling mashr function `cov_canonical` with its default settings. This collection of covariance matrices included covariances capturing independent effects across all conditions (identity matrix); equal effects across all conditions (a matrix of ones); and condition-specific effects.
- (b) *Estimate data-driven covariance matrices.* Additionally, we estimated 6 data-driven covariance matrices using the Extreme Deconvolution (ED) method ([Bovy et al., 2011](#)). ED is included with mashr and called via the mashr function `cov_ed`. The ED estimates were initialized from a PCA of the effect estimates: a rank-5 covariance matrix defined by the top 5 PCs; and 5 rank-1 matrices each defined by one of the top 5 PCs. This was accomplished by calling mashr function `cov_pca` with `npc = 5`. Both initial covariance estimates (via `cov_pca`) and final covariance estimates (via `cov_ed`) were obtained using only the strongest signals; that is, genes j with $lfsr < 0.05$ in at least one condition as determined by a simple condition-by-condition analysis implemented in the ashr R package ([Stephens, 2017](#)). Note that the ED updates are “subspace preserving”; when the ED estimates are initialized as rank-1 matrices, the final estimates are also rank-1.
- (c) *Modify data-driven covariance matrices.* To deal with the issue that the $lfsr$ can be underestimated when low-rank prior covariance matrices are used, we added a small scalar, $0.01 \times a_k$, to the diagonal of each data-driven covariance matrix \mathbf{U}_k , in which a_k was the maximum value along the diagonal of \mathbf{U}_k .
- (d) *Determine scaling coefficients.* The mash prior also requires specification of the scaling coefficients w_l , and for this we used the automated selection of scaling coefficients implemented in mashr.
- (v) *Fit mash model.* We fit the mash model and computed posterior quantities by calling the `mash` function from mashr, in which all optional arguments were kept at their defaults. The

one exception is that we set `alpha = 1` in `mash_set_data`, which specifies the “exchangeable z -scores” (EZ) model (Stephens, 2017; Urbut et al., 2019). In initial trials, we found that the EZ model performed better than the “exchangeable effects” (EE) model.

- (vi) *Detect expression differences.* We reported expression differences for gene-condition pairs based on the `lfsr`, and we identified differentially expressed genes based on the *minimum lfsr*.

F.1.6 Poisson mash

The Poisson mash analysis pipeline was modeled after the mash analysis pipeline. We took the following steps to fit a Poisson mash model (or Poisson mash RUV model) and compute key posterior quantities. Some steps were specific to the Poisson mash RUV model. All steps were implemented in the `poisson.mash.alpha` R package (version 0.1-87).

- (i) *Compute size factors.* We computed the cell-specific size factors \tilde{s}_i from \mathbf{Y} by calling function `calculateSumFactors` from the `scrn` R package, in which clusters were determined by running the `quickCluster` function on \mathbf{Y} .
- (ii) *Aggregate single-cell data.* We summed the UMI counts \mathbf{Y} across cells by condition to obtain condition-level counts \mathbf{X} . This step was implemented in function `pois_mash_set_data`.
- (iii) *Estimate unwanted variation from single-cell data (Poisson mash RUV only).* We estimated the $J \times D$ matrix \mathbf{F} by fitting a GLM-PCA model to \mathbf{Y} using the algorithms implemented in the `glmpca` package (version 0.2.0.9000; Townes et al. 2019; Townes and Street 2021). Specifically, we fit a GLM-PCA model with negative-binomial likelihood (`fam = "nb2"`) and with a separate overdispersion parameter for each gene. We included the R conditions as covariates in the GLM-PCA model. We used $D = 4$ factors for the smaller simulated data sets and $D = 5$ factors for the larger data sets.
- (iv) *Get initial parameter estimates.* To get sensible initial estimates of the parameters $\boldsymbol{\mu}$ and $\boldsymbol{\psi}$ (and $\boldsymbol{\rho}$ for Poisson mash RUV), we fit the Poisson mash model with the assumption that there were no differences in expression among the conditions; that is, $\beta_{jr} = 0$ for all $j = 1, \dots, J$, $r = 1, \dots, R$. Without expression differences, the mash prior is not needed, which simplifies estimation. These initial parameter estimates were then used to initialize subsequent model fitting. This step was implemented by function `pois_mash_ruv_pfit`.
- (v) *Determine covariance matrices in mash prior.* Like mash, we defined the covariance matrices \mathbf{U}_k in the mixture prior in a separate step before fitting the full Poisson mash model. As in mash, we included a mixture of canonical and data-driven matrices in the prior. In total, we included $K = R + 7$ covariance matrices.
 - (a) *Define canonical covariance matrices.* For the canonical matrices, we included only the matrices capturing condition-specific effects. We did not include the “independent effects” matrix (the identity matrix) because it is not needed when the random effect is included. We did not include the “equal effects” matrix (a matrix of ones) since the μ_j ’s already perform a similar role.

- (b) *Get initial estimates of data-driven covariance matrices.* As in the mash analysis pipeline, the data-driven covariance matrices were estimated using a two-step process: an initialization phase followed by a refinement phase. The initialization was performed by function `pois_cov_init`, and is analogous to the `cov_pca` step in the mash analysis pipeline (and indeed `pois_cov_init` uses PCA in a very similar way to `cov_pca`). Instead of computing PCs using the limma effect estimates, we computed PCs using the z -scores from a multinomial goodness-of-fit test. Specifically, for a given gene j , we tested whether $\lambda_{jr} = \lambda_j$ for all conditions $r = 1, \dots, R$. As in the mash analysis pipeline, we only used the genes j containing “strong signals.” We selected strong signals based on the z -scores from the multinomial goodness-of-fit test; specifically, genes with at least one z -score greater than 3 in magnitude.
- (c) *Refine estimates of data-driven covariance matrices.* The refinement phase was implemented in function `pois_cov_ed` and is analogous to the `cov_ed` function in mash (noting that the function `pois_cov_ed` is confusingly named and does not actually use Extreme Deconvolution). To refine the data-driven covariance matrices, we fit a simplified Poisson mash (or Poisson mash RUV) model without the scaling factors (i.e., $L = 1$, $w_1 = 1$). As in the initialization phase, only the genes with the strongest signals were used.
- (d) *Modify data-driven covariance matrices.* Similar to the mash pipeline, after rescaling each \mathbf{U}_k so that the largest entry along the diagonal was 1, we added a small constant, $\epsilon = 0.01$, to the diagonal entries of the data-driven covariance matrices. This was done to avoid possible issues with $lfsr$ calculations.
- (e) *Determine scaling factors in mash prior.* The mash prior also includes scaling factors w_l to allow for a wide range of effect sizes. We used the automated setting of the scaling factors implemented in the `pois_mash` function. In brief, `pois_mash` chooses an evenly spaced grid of scaling factors, in which the range is determined dynamically by the data. A maximum-likelihood estimate of λ_{jr} was computed for each gene j and condition r by $\hat{\lambda}_{jr} = (x_{jr} + 0.1)/s_r$ (a pseudocount of 0.1 was added to avoid logarithms of zero). Then the range of the scaling factors was chosen based on the range of $\log \hat{\lambda}_{jr}$. We set `gridmult = 2.5` so that the scaling factors were spaced (multiplicatively) by a factor of 2.5.
- (vi) *Fit Poisson mash model.* We called `pois_mash` to fit the Poisson mash (or Poisson mash RUV) model. This function fits the model by iterating the variational EM updates. We ran at most 300 model fitting iterations.
- (vii) *Detect expression differences.* Finally, we reported a gene-condition pair j, r as having an expression difference if the $lfsr$ outputted by `pois_mash` was less than a specified threshold. We reported differentially expressed genes as those in which the *minimum* $lfsr$ was less than a specified threshold.

F.2 Bulk RNA-seq data simulations with multiple replicates

We took the following steps to simulate bulk RNA-seq data sets. We generated RNA-seq count data for $4 \times R$ samples measured in 10,000 genes using the function `generateSyntheticData` from the R package `compcoder` (Soneson, 2014). This function simulates the count for gene j in sample i

from a negative binomial distribution with mean parameter $s_i \frac{\mu_j}{\sum_{j=1}^m \mu_j}$ and dispersion parameter ϕ_j , independently across samples and genes. The sequencing depth s_i for sample i was drawn uniformly from the interval $[0.7 \times 10^7, 1.4 \times 10^7]$, and μ_j, ϕ_j were randomly drawn from paired values estimated from real data (Pickrell et al., 2010; Cheung et al., 2010). Next, we randomly assigned each of the $4 \times R$ samples to one of the R conditions so that there were 4 replicate samples per condition and no systematic expression differences among the conditions. Finally, we used binomial thinning (Gerard, 2020) to simulate expression differences in 1,000 randomly chosen genes as was described in Section 6.1 of the main text.

For each setting of R , we followed this procedure to simulate 20 data sets.

F.3 Computing environment

All analyses of simulated and real data sets were performed in R 4.1.0 (R Core Team, 2021), linked to the OpenBLAS 0.3.13 optimized numerical libraries, on Linux machines (Scientific Linux 8) with Intel Xeon E5-2680v4 (“Broadwell”) processors. Note that fitting the Poisson mash models to the larger cytokines data sets required more memory, as much as 100 GB, and for these larger data sets we also used multithreading to speed up the computations (at most 3 cores).

Appendix G Cytokines experiment protocols and data preparation

G.1 Mice samples

Female C57BL/6J mice (Strain #000664) were obtained from Jackson Laboratories. Age-matched female mice (6 to 8 weeks old) were used in all experiments. Animals were housed in specific pathogen-free and BSL2 conditions at the University of Chicago. All experiments were performed in accordance with the US National Institutes of Health Guide for the Care and Use of Laboratory Animals and approved by the University of Chicago Institutional Animal Care and Use Committee.

G.2 Library preparation

Mice were intravenously injected with 2.5 μ g of the following 48 recombinant cytokines: IL-1 β (211-11B), IL-2 (212-12), IL-3 (213-13), IL-4 (214-14), IL-5 (215-15), IL-6 (216-16), IL-7 (217-17), IL-9 (219-19), IL-10 (210-10), IL-11 (220-11), IL-12 p70 (210-12), IL-13 (210-13), IL-15 (210-15), IL-17A (210-17), IL-17F (210-17F), IL-21 (210-21), IL-22 (210-22), IL-33 (210-33), IFN- γ (315-05), M-CSF (315-02), GM-CSF (315-03), G-CSF (250-05), TNF (315-01A), TGF- β 1 (100-21), CCL2 (250-10), CCL3 (250-09), CCL4 (250-32), CCL11 (250-01), CCL17 (300-30), CCL20 (250-27), CCL22 (250-23), CXCL1 (250-11), CXCL5 (300-22), CXCL9 (250-18), CXCL10 (250-16), CXCL12 (250-20A), CXCL13 (250-24) (purchased from Peprotech), IFN- α 1 (751802), IFN- β (581302) (purchased from BioLegend), IL-1 α (400-ML-025), IL-18 (9139-IL-010), IL-23 (1887-ML-010), IL-25 (7909-IL-010), IL-27 (2799-ML-010), IL-34 (5195-ML-010), IL-36 α (7059-ML-010), CCL5 (478-MR-025), and TSLP (555-TS-010) (purchased from R&D Systems). Untreated mice were used as a control. Three mice were used for each cytokine treatment group and control group. Mice were anesthetized with avertin (250-500 mg/kg) 12 h after cytokine injection and whole blood was collected from the left ventricle of the heart into the tubes containing ice-cold buffer (PBS plus 0.5% FCS and 2 mmol/L EDTA). Red blood cells were lysed in ACK Red blood cell lysis buffer (Lonza, BW10548E) for 3 min and then 3 biological replicates per treatment group were pooled into a tube. After pooling samples,

the cells were washed by the buffer. Anti-Ter119 MicroBeads (Miltenyi Biotec, 130-049-901) was used to deplete Ter119⁺ cells thoroughly. Cells were then labeled with the TotalSeqTM-C0301 anti-mouse Hashtag 1 antibody (BioLegend, 155861) and TotalSeqTM-C0302 anti-mouse Hashtag 2 antibody (BioLegend, 155863) at 0.25 $\mu\text{g}/\text{sample}$ for 15 min at 4 °C. After staining, cells were washed with PBS, and resuspended in PBS + 0.04% BSA. Cells were counted and resuspended at a density of 1000 cells/ μL .

Cell capture and library preparations were performed using the 10x Genomics Chromium controller, the Chromium Single Cell 5' Library & Gel Bead Kit (10x Genomics, PN-1000006), the Chromium Single Cell 5' Feature Barcode Library Kit (10x Genomics, PN-1000080), the Chromium Chip A Single Cell Kit (10x Genomics, PN-120236), the Chromium i7 Multiplex Kit (10x Genomics, PN-120262), and the Chromium i7 Multiplex Kit N, Set A (10x Genomics, PN-1000084) according to the manufacturer's protocol. Libraries were loaded onto a NextSeq 500/550 High Output Kit v2.5 (75 Cycles) (Illumina, 20024906). Hashtag indexing was used for demultiplexing the sequencing data. Sequencing was done in two batches, with 3 cytokine treatments (TNF, IFN- α 1, IFN- β) plus one control in the first batch and 45 cytokine treatments plus one control in the second batch.

In our analyses, we used only the data from the second batch to avoid batch effects. We also excluded the IL-27 due to a technical issue in the experiment.

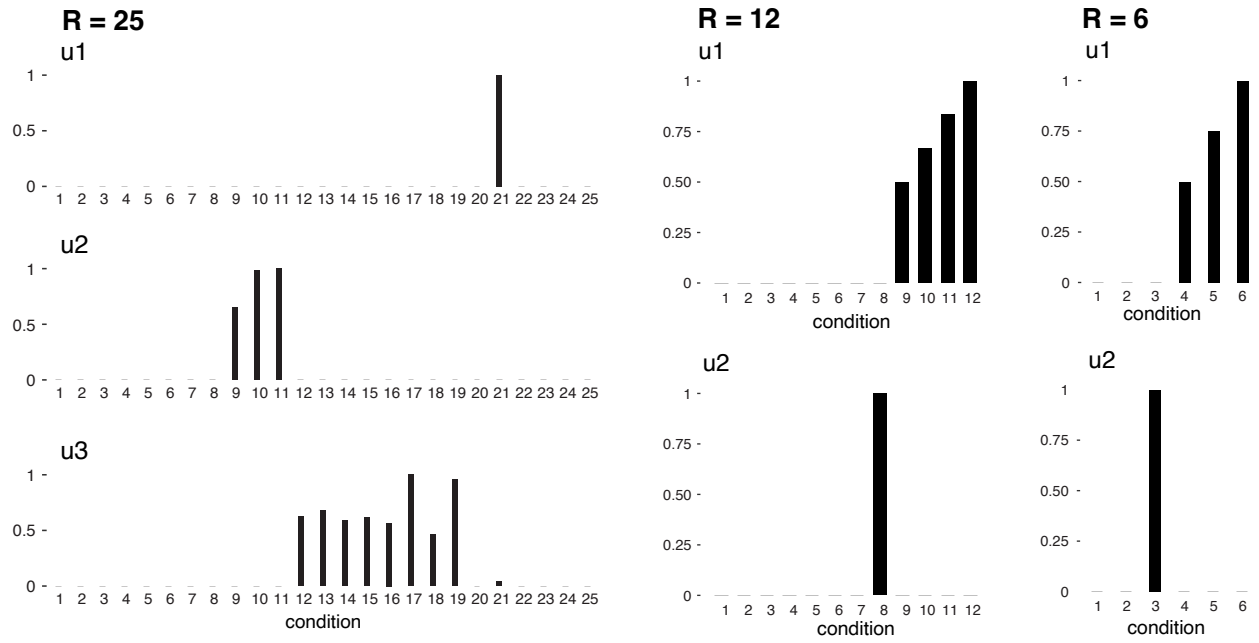
G.3 Raw read processing

Raw sequencing data were processed by the Cell Ranger pipeline (Zheng et al., 2017) to produce UMI counts. Quality control steps were taken to filter out cells with too low (<400) or high (>22,000) counts, as well as cells with a large fraction of mitochondrial counts (>20%).

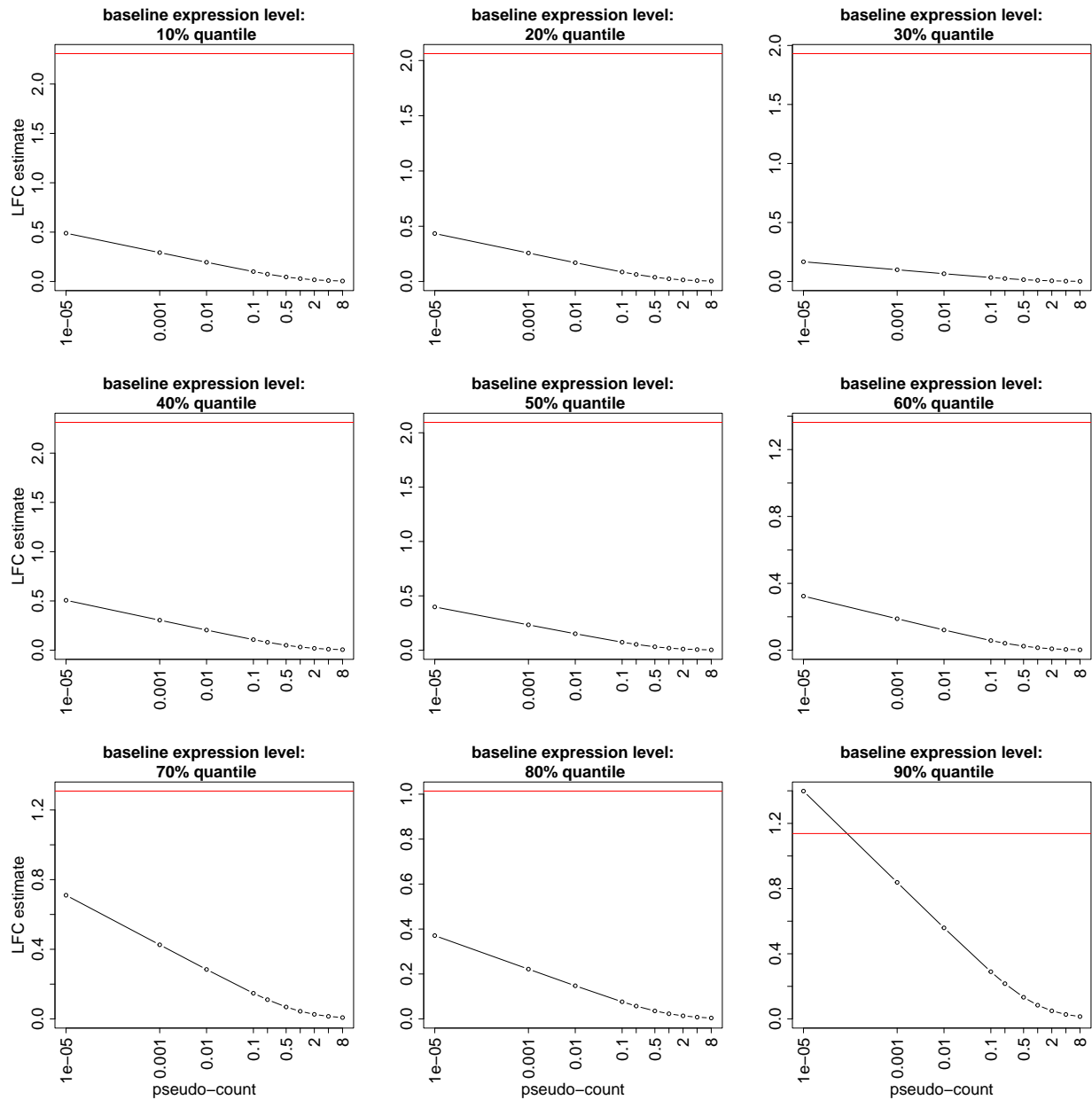
Cells were assigned to cell types by clustering using the Louvain algorithm (Blondel et al., 2008). Based on known marker genes, we annotated 8 of the clusters as cell types: B cells (*Cd19*, *Cd79a*, *Cd79b*); CD4⁺ T cells (*Cd3d*, *Cd3e*, *Thy1*, *Cd4*), CD8⁺ T cells (*Cd3d*, *Cd3e*, *Thy1*, *Cd8a*); dendritic cells (*Flt3*); Ly6C⁻ monocytes (*Nr4a1*, *Pparg*); Ly6C⁺ monocytes (*Ly6c2*, *F13a1*), neutrophils (*S100a8*, *S100a9*); and natural killer (NK) cells (*Ncr1*). For a given cell type, genes expressed in fewer than 20 cells were removed.

The processed data used in the Poisson mash analyses is summarized in Supplementary Table S1 and in the Supplementary Data.

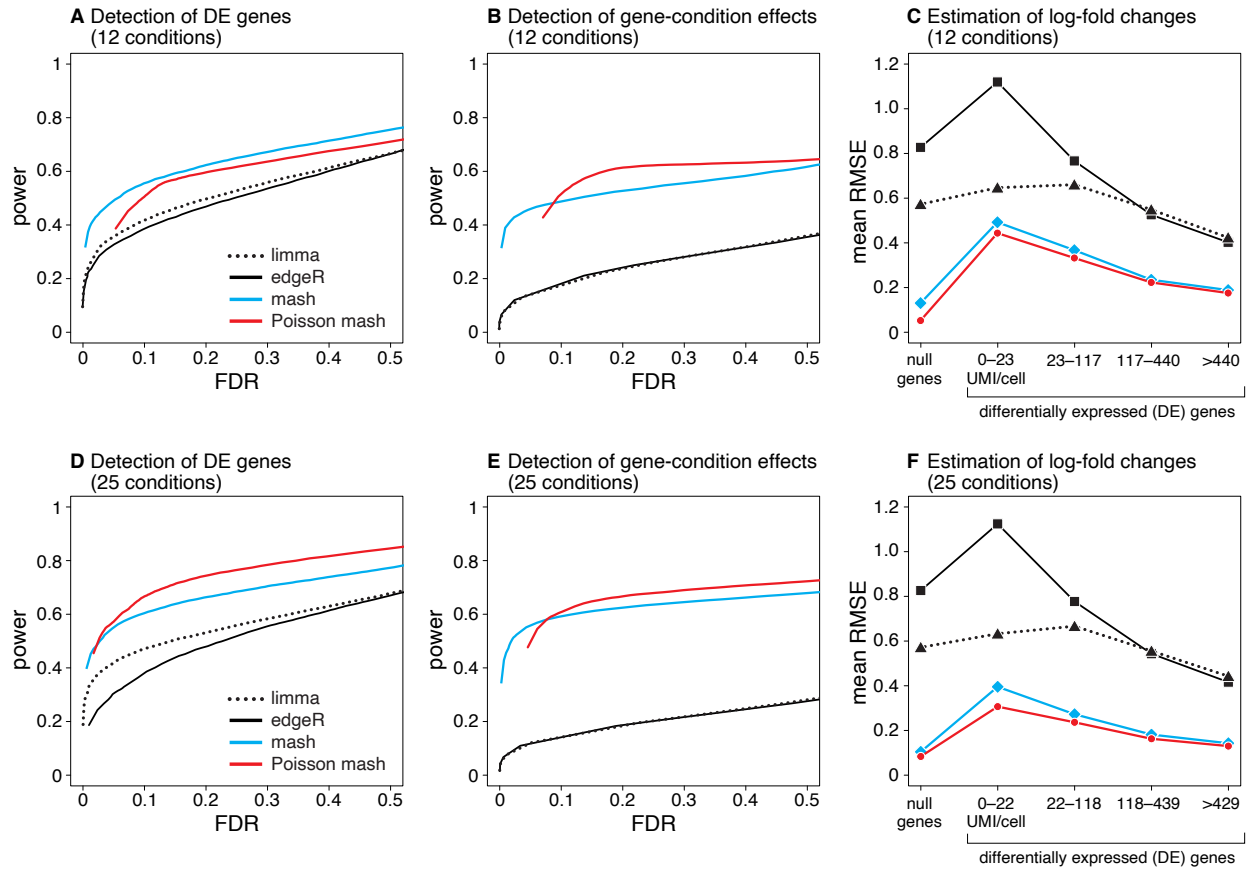
Supplementary figures.



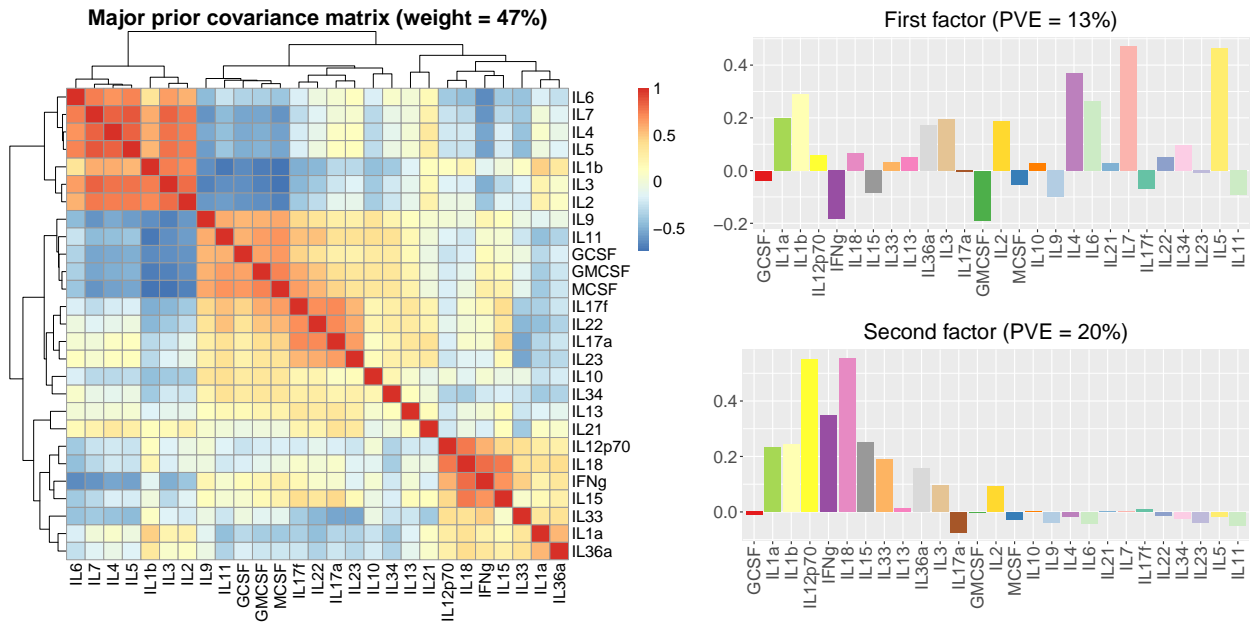
Supplementary Figure S1: Cross-condition sharing patterns used to simulate the treatment effects for data sets simulated with $R = 25, 12$ and 6 .



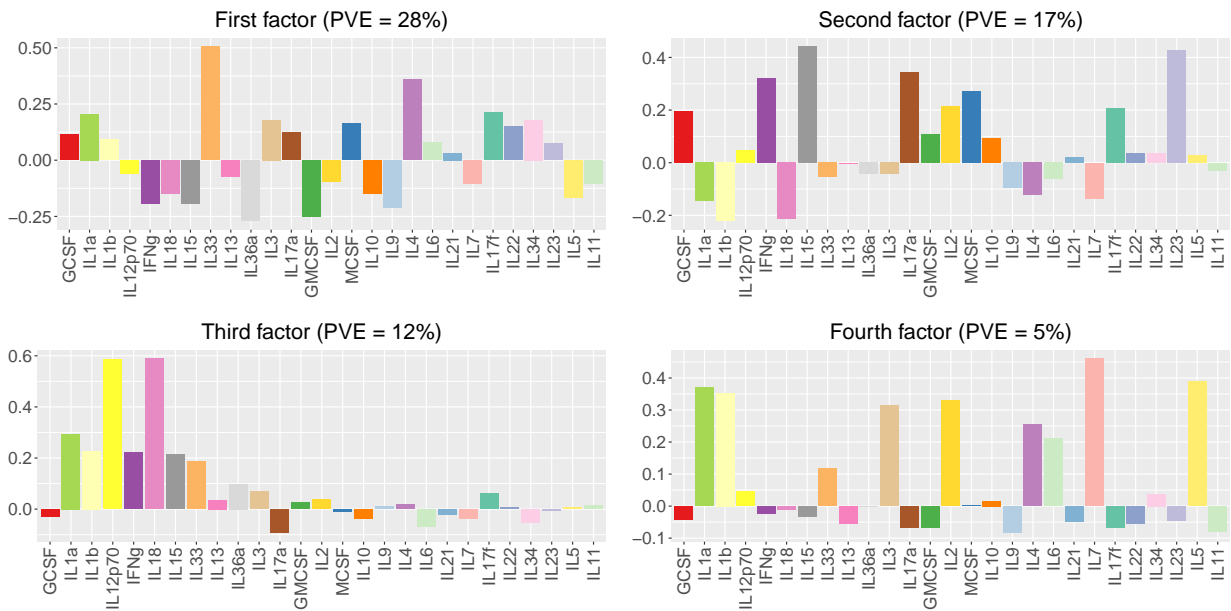
Supplementary Figure S2: Illustration of impact of pseudocount on LFC estimation bias. Results show the LFC estimate obtained using limma (circles, joined by black line) against the truth (red horizontal line) for different choices of pseudocount. The 9 panels show results for 9 DE gene-condition pairs chosen from a simulated data set in the larger sample size scenario, with the genes ordered by their baseline expression level. These results are consistent with [Lun \(2018\)](#) who showed that differences in log-transformed expression values (with pseudocount) between conditions often do not accurately estimate the LFC, especially when counts are low.



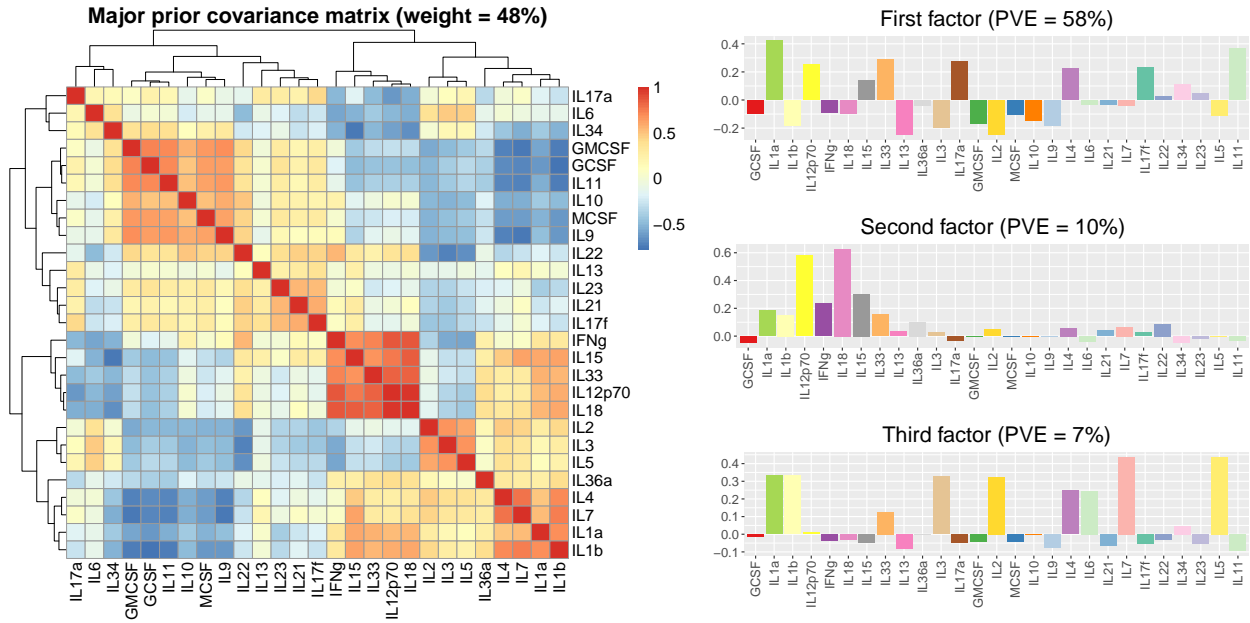
Supplementary Figure S3: Evaluation of DE analysis methods in simulated bulk RNA-seq data sets, $R = 12$ conditions (top row) and $R = 25$ conditions (bottom row). FDR and power were calculated for all genes (Panels A, D) and for all gene-condition pairs (B, E) in the 20 simulations by varying a p -value or $lfsr$ threshold from 0 to 1. Panels C and F summarize LFC estimation accuracy by the RMSE, averaged over 20 simulations. RMSE was calculated in non-overlapping groups of genes: “null” genes (genes in which there were no differences in expression in all conditions); and DE genes grouped by expression level (read counts per sample).



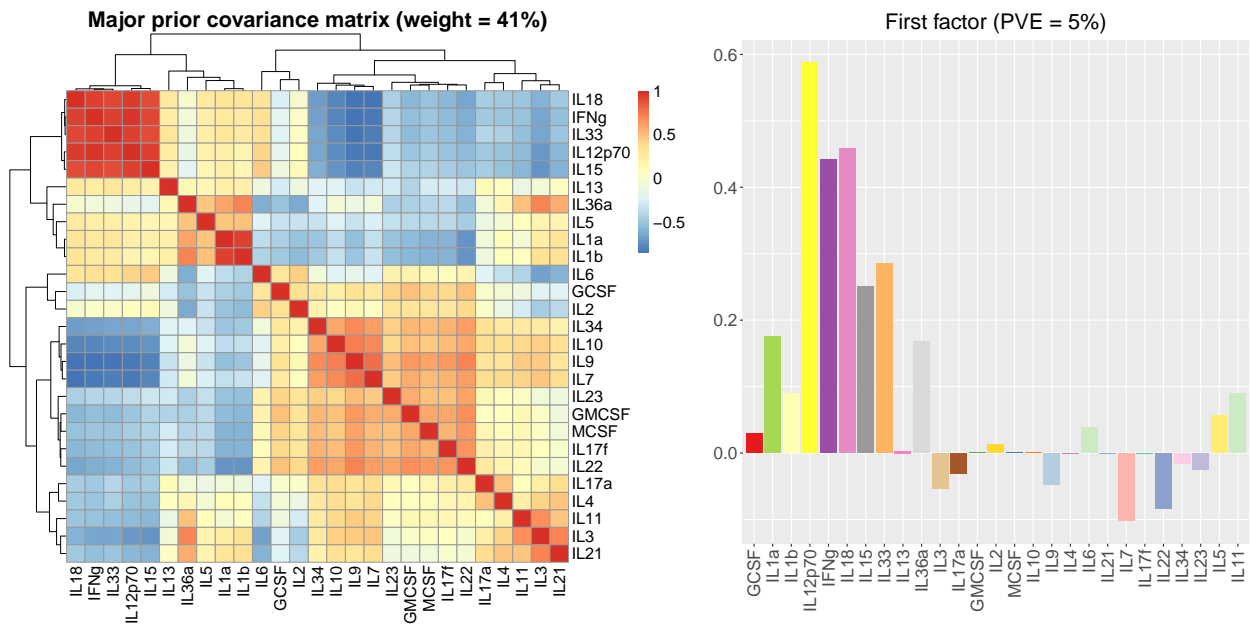
Supplementary Figure S4: Poisson mash RUV estimates of prior (left) and posterior (right) patterns of differential expression across cytokine treatments in B cells. Left panel shows a heatmap of the correlation matrix of the prior covariance matrix that receives the largest weight in the Poisson mash RUV fit. Right panel shows the top factors by PVE from a factor analysis of the posterior mean LFC estimates.



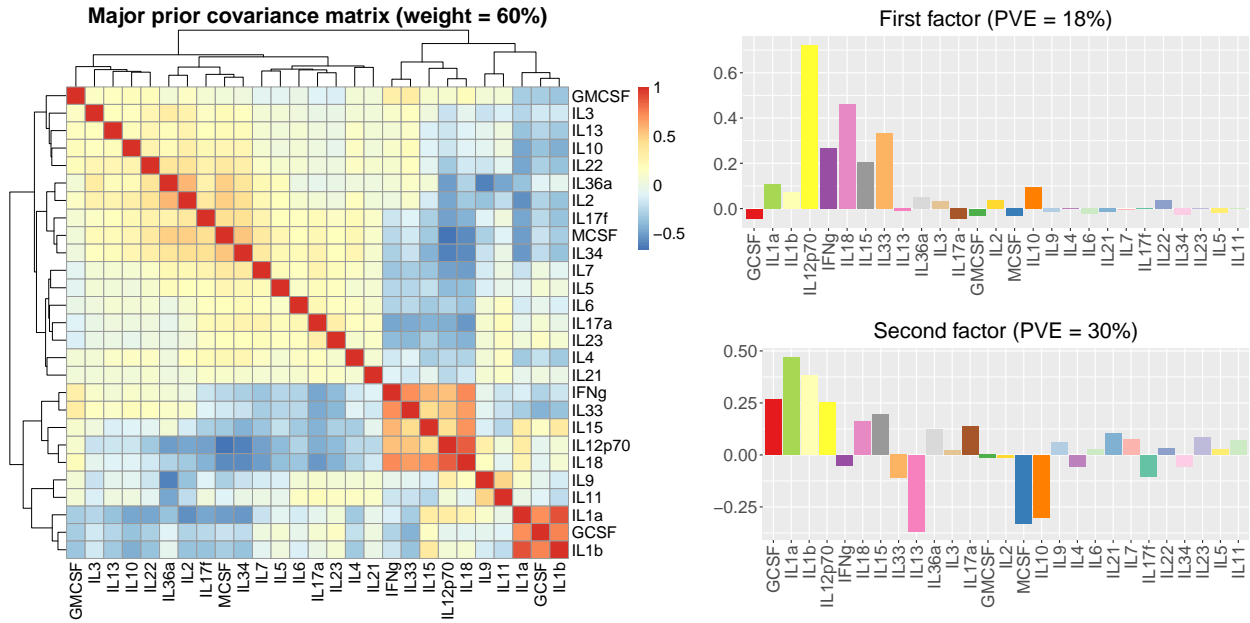
Supplementary Figure S5: Poisson mash RUV estimates of posterior patterns of differential expression across cytokine treatments in CD4⁺ T cells. The top factors by PVE from a factor analysis of the posterior mean LFC estimates are shown.



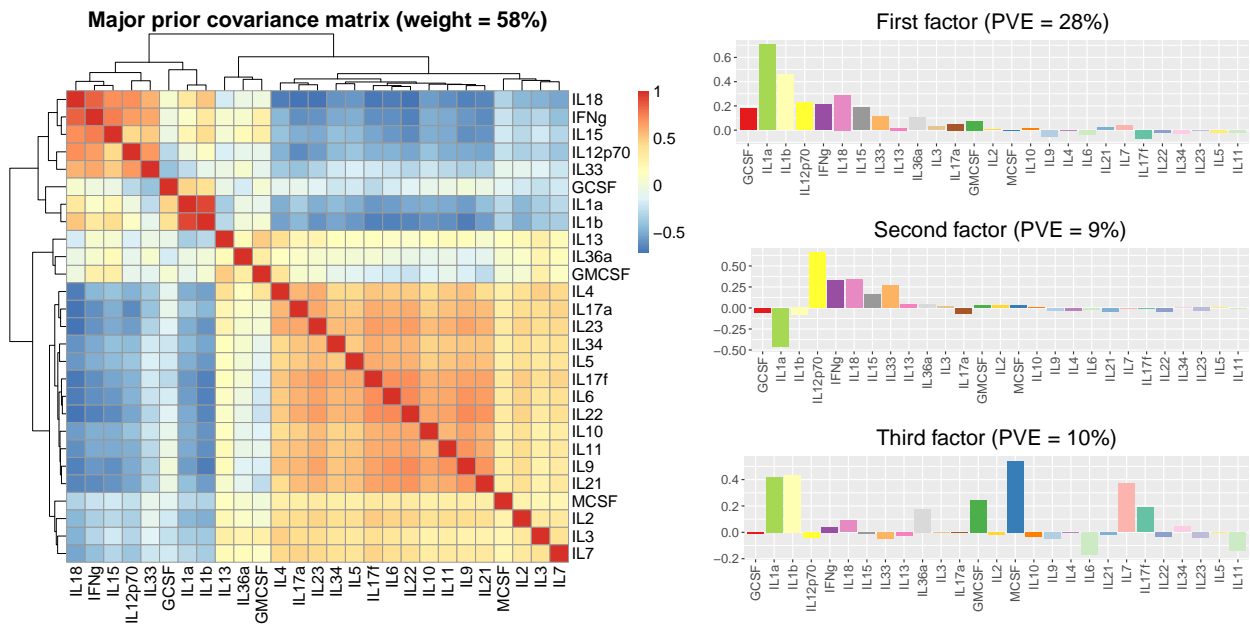
Supplementary Figure S6: Poisson mash RUV estimates of prior (left) and posterior (right) patterns of differential expression across cytokine treatments in CD8⁺ T cells. Left panel shows a heatmap of the correlation matrix of the prior covariance matrix that receives the largest weight in the Poisson mash RUV fit. Right panel shows the top factors by PVE from a factor analysis of the posterior mean LFC estimates.



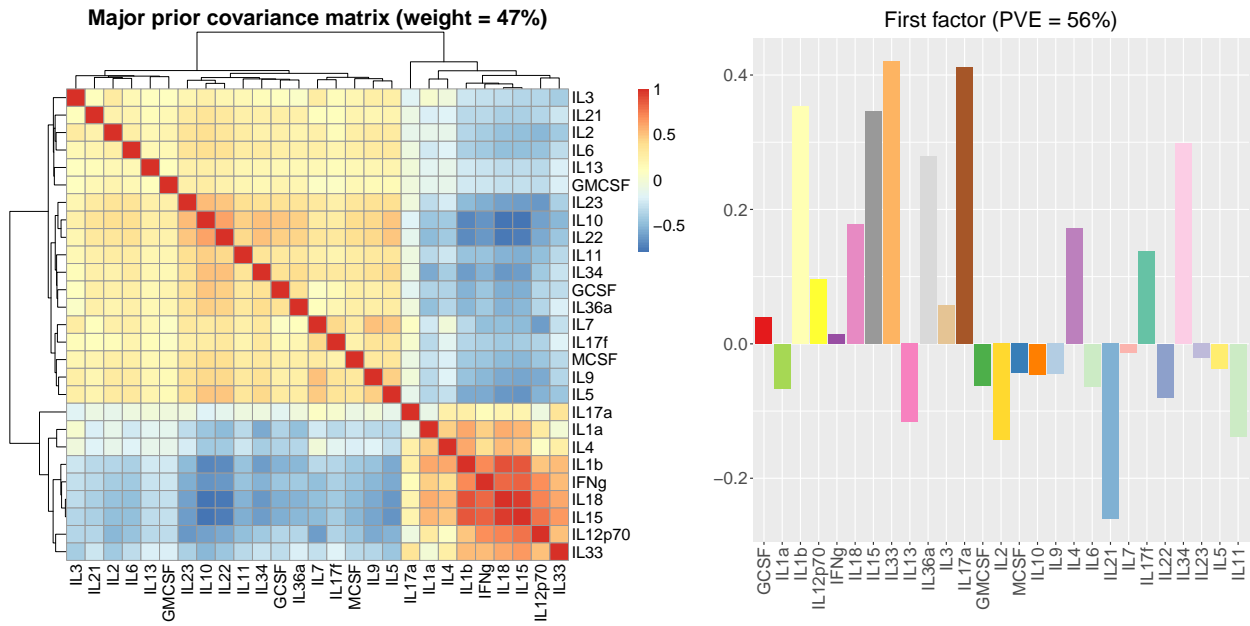
Supplementary Figure S7: Poisson mash RUV estimates of prior (left) and posterior (right) patterns of differential expression across cytokine treatments in dendritic cells. Left panel shows a heatmap of the correlation matrix of the prior covariance matrix that receives the largest weight in the Poisson mash RUV fit. Right panel shows the top factor by PVE from a factor analysis of the posterior mean LFC estimates.



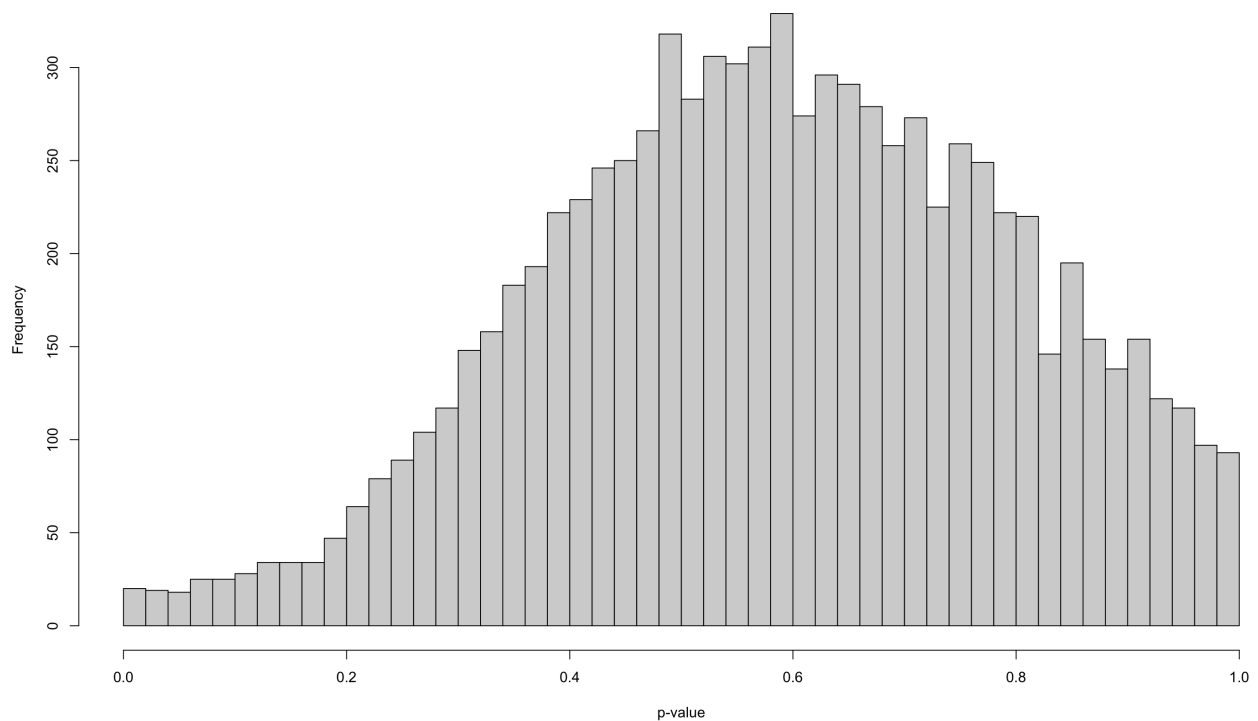
Supplementary Figure S8: Poisson mash RUV estimates of prior (left) and posterior (right) patterns of differential expression across cytokine treatments in Ly6C⁻ monocytes. Left panel shows a heatmap of the correlation matrix of the prior covariance matrix that receives the largest weight in the Poisson mash RUV fit. Right panel shows the top factors by PVE from a factor analysis of the posterior mean LFC estimates.



Supplementary Figure S9: Poisson mash RUV estimates of prior (left) and posterior (right) patterns of differential expression across cytokine treatments in Ly6C⁺ monocytes. Left panel shows a heatmap of the correlation matrix of the prior covariance matrix that receives the largest weight in the Poisson mash RUV fit. Right panel shows the top factors by PVE from a factor analysis of the posterior mean LFC estimates.



Supplementary Figure S10: Poisson mash RUV estimates of prior (left) and posterior (right) patterns of differential expression across cytokine treatments in NK cells. Left panel shows a heatmap of the correlation matrix of the prior covariance matrix that receives the largest weight in the Poisson mash RUV fit. Right panel shows the top factor by PVE from a factor analysis of the posterior mean LFC estimates.



Supplementary Figure S11: Assessment of goodness-of-fit of the Poisson mash RUV model fit to the neutrophils data. The histogram shows the empirical distribution of p -values from the goodness-of-fit tests for 8,543 genes.

Supplementary tables.

Supplementary Table S1: Summary of the processed cytokine stimulation data. “Median total UMI count” is the median of the cell-wise total UMI counts.

cell type	cells	median total UMI count	genes
B cells	87,140	1,789	11,698
CD4 ⁺ T cells	12,939	1,971	10,462
CD8 ⁺ T cells	14,282	2,791	10,819
dendritic cells	778	6,255	8,952
Ly6C ⁻ monocytes	3,677	3,824	10,236
Ly6C ⁺ monocytes	4,229	5,269	10,404
neutrophils	13,362	1,127	8,543
natural killer cells	1,735	2,194	8,496

Supplementary Table S2: Patterns of differential expression shared across cell types based on Gene Ontology (GO) gene set enrichment analyses. To generate the GO enrichment results using WebGestalt (Liao et al., 2019; Ashburner et al., 2000; The Gene Ontology Consortium, 2020), we first performed, for each cell type, a factor analysis (Wang and Stephens, 2021) on the $N_{de} \times 27$ matrix of posterior mean LFCs from the N_{de} genes that were identified as differentially expressed by Poisson mash RUV in that cell type. We defined the “driving genes” for a factor as all genes with $lfsr < 0.001$, then we split the driving genes into two sets based on whether the factor estimate was positive or negative. We performed two GO gene set enrichment analyses for each factor: one for the positive driving genes, and one for the negative driving genes. The table lists the results for all “significantly enriched” GO gene sets which we defined as gene sets with a false discovery rate (FDR) less than 0.05. Columns in the table from left-to-right are: the cytokine conditions with the largest factor values; the cell types in which the factors were identified; whether the enrichment was based on the positive or negative driving genes; and the significantly enriched GO gene sets.

top cytokines	cell types	direction of regulation	significant GO terms
IL12p70, IL18, IFNg, IL15, IL33	B cells, CD4 T cells, CD8 T cells, Ly6C- monocytes, Ly6C+ monocytes, neutrophils	+	response to interferon-beta, response to interferon-gamma, response to virus, antigen processing and presentation, regulation of innate immune response, regulation of immune effector process, defense response to bacterium, positive regulation of defense response, positive regulation of cytokine production, regulation of response to cytokine stimulus
IL33, IL4	CD4 T cells,		chromosome localization, chromosome segregation, microtubule cytoskeleton organization
IL12p70, IL17a, IL17f, IL1a, IL4, IL11, IL15, IL33	CD8 T cells	+	involved in mitosis, spindle organization, organelle fission, regulation of chromosome organization, DNA conformation change, regulation of mitotic cell cycle, positive regulation of cell cycle, cell cycle phase transition
IL17a, IL15, IL1b, IL33, IL34, IL36a	NK cells NK cells		
IL1a, IL1b, IL2, IL3, IL4, IL5, IL6, IL7	B cells, CD4 T cells, CD8 T cells	+	cytoplasmic translation, ribonucleoprotein complex subunit organization, ncRNA metabolic process, ribonucleoprotein complex biogenesis
IL12p70, IL15, IL18, IFNg, IL33	dendritic cells, Ly6C+ monocytes	-	

Supplementary Table S3: Cell-type-specific patterns of differential expression based on Gene Ontology (GO) gene set enrichment analyses. See Supplementary Table S2 for details.

top cytokines	cell type	direction of regulation	significant GO terms
IL1a, IL1b, IL2, IL3, IL4, IL5, IL6, IL7	B cells	-	digestive system development, peptidyl-threonine modification, embryonic organ development, cell-cell signaling by wnt, protein acylation, peptidyl-serine modification, cell surface receptor signaling pathway involved in cell-cell signaling, covalent chromatin modification, peptidyl-lysine modification
IL15, IFNg, IL23, IL17a, IL17f, GCSF, MCSF	CD4 T cells	+	coagulation, homotypic cell-cell adhesion, regulation of tube size, regulation of body fluid levels, response to wounding, fatty acid metabolic process
IL1a, IL1b, GCSF, IL12p70	Ly6C- monocytes	+	humoral immune response, response to interleukin-1, negative regulation of proteolysis, regulation of vasculature development, cell chemotaxis, regulation of peptidase activity
IL1a, IL1b, GCSF, IL12p70, IL15, IL18, IFNg	Ly6C+ monocytes	+	mitochondrial gene expression, protein folding, protein localization to mitochondrion, nucleoside monophosphate metabolic process, nucleoside triphosphate metabolic process, generation of precursor metabolites and energy, purine-containing compound metabolic process, ribose phosphate metabolic process
IL1a, IL1b, GCSF	neutrophils	+	morphogenesis of a polarized epithelium, regulation of synapse structure or activity, cell junction organization, transition metal ion homeostasis, synapse organization, positive regulation of cytoskeleton organization, actin filament organization, regulation of supramolecular fiber organization, regulation of actin filament-based process, regulation of inflammatory response

References

- Ahlmann-Eltze, C. and Huber, W. (2020). glmGamPoi: fitting Gamma-Poisson generalized linear models on single cell count data. *Bioinformatics*, 36(24):5701–5702.
- Aitchison, J. and Ho, C. (1989). The multivariate Poisson-log normal distribution. *Biometrika*, 76(4):643–653.
- Altmeier, S., Toska, A., Sparber, F., Teixeira, A., Halin, C., and LeibundGut-Landmann, S. (2016). IL-1 coordinates the neutrophil response to *C. albicans* in the oral mucosa. *PLoS Pathogens*, 12(9):e1005882.
- Anders, S. and Huber, W. (2010). Differential expression analysis for sequence count data. *Genome Biology*, 11:R106.
- Arridge, S. R., Ito, K., Jin, B., and Zhang, C. (2018). Variational Gaussian approximation for Poisson data. *Inverse Problems*, 34(2):025005.
- Ashburner, M., Ball, C. A., Blake, J. A., Botstein, D., Butler, H., Cherry, J. M., Davis, A. P., Dolinski, K., Dwight, S. S., Eppig, J. T., Harris, M. A., Hill, D. P., Issel-Tarver, L., Kasarskis, A., Lewis, S., Matese, J. C., Richardson, J. E., Ringwald, M., Rubin, G. M., and Sherlock, G. (2000). Gene Ontology: tool for the unification of biology. *Nature Genetics*, 25(1):25–29.
- Blei, D. M., Kucukelbir, A., and McAuliffe, J. D. (2017). Variational inference: a review for statisticians. *Journal of the American statistical Association*, 112(518):859–877.
- Blondel, V. D., Guillaume, J.-L., Lambiotte, R., and Lefebvre, E. (2008). Fast unfolding of communities in large networks. *Journal of Statistical Mechanics: Theory and Experiment*, 2008(10):P10008.
- Bochkina, N. and Richardson, S. (2007). Tail posterior probability for inference in pairwise and multiclass gene expression data. *Biometrics*, 63(4):1117–1125.
- Boothby, I. C., Cohen, J. N., and Rosenblum, M. D. (2020). Regulatory T cells in skin injury: at the crossroads of tolerance and tissue repair. *Science Immunology*, 5(47):eaaz9631.
- Bovy, J., Hogg, D. W., and Roweis, S. T. (2011). Extreme deconvolution: inferring complete distribution functions from noisy, heterogeneous and incomplete observations. *Annals of Applied Statistics*, 5(2B):1657–1677.
- Bullard, J. H., Purdom, E., Hansen, K. D., and Dudoit, S. (2010). Evaluation of statistical methods for normalization and differential expression in mRNA-Seq experiments. *BMC Bioinformatics*, 11:94.
- Chang, J., Burkett, P. R., Borges, C. M., Kuchroo, V. K., Turka, L. A., and Chang, C.-H. (2013). MyD88 is essential to sustain mTOR activation necessary to promote T helper 17 cell proliferation by linking IL-1 and IL-23 signaling. *Proceedings of the National Academy of Sciences*, 110(6):2270–2275.

- Chen, Y., Lun, A., and Smyth, G. (2016). From reads to genes to pathways: differential expression analysis of RNA-seq experiments using Rsubread and the edgeR quasi-likelihood pipeline [version 2; peer review: 5 approved]. *F1000Research*, 5:1438.
- Cheung, V. G., Nayak, R. R., Wang, I. X., Elwyn, S., Cousins, S. M., Morley, M., and Spielman, R. S. (2010). Polymorphic cis-and trans-regulation of human gene expression. *PLoS Biology*, 8(9):e1000480.
- Cooper, A. M., Magram, J., Ferrante, J., and Orme, I. M. (1997). Interleukin 12 (IL-12) is crucial to the development of protective immunity in mice intravenously infected with Mycobacterium tuberculosis. *Journal of Experimental Medicine*, 186(1):39–45.
- Cover, T. M. and Thomas, J. A. (2006). *Elements of Information Theory*. Wiley, Hoboken, NJ, 2nd edition.
- Crowell, H. L., Soneson, C., Germain, P.-L., Calini, D., Collin, L., Raposo, C., Malhotra, D., and Robinson, M. D. (2020). muscat detects subpopulation-specific state transitions from multi-sample multi-condition single-cell transcriptomics data. *Nature Communications*, 11:6077.
- Cruz, A., Khader, S. A., Torrado, E., Fraga, A., Pearl, J. E., Pedrosa, J., Cooper, A. M., and Castro, A. G. (2006). Cutting edge: IFN- γ regulates the induction and expansion of IL-17-producing CD4 T cells during mycobacterial infection. *Journal of Immunology*, 177(3):1416–1420.
- Dinarello, C. A. (2018). Overview of the IL-1 family in innate inflammation and acquired immunity. *Immunological Reviews*, 281(1):8–27.
- Dinarello, C. A., Simon, A., and Van Der Meer, J. W. (2012). Treating inflammation by blocking interleukin-1 in a broad spectrum of diseases. *Nature Reviews Drug Discovery*, 11(8):633–652.
- Dreis, C., Ottenlinger, F. M., Putyrski, M., Ernst, A., Huhn, M., Schmidt, K. G., Pfeilschifter, J. M., and Radeke, H. H. (2019). Tissue cytokine IL-33 modulates the cytotoxic CD8 T lymphocyte activity during nutrient deprivation by regulation of lineage-specific differentiation programs. *Frontiers in Immunology*, page 1698.
- Erdmann-Pham, D. D., Fischer, J., Hong, J., and Song, Y. S. (2021). Likelihood-based deconvolution of bulk gene expression data using single-cell references. *Genome Research*, 31(10):1794–1806.
- Finak, G., McDavid, A., Yajima, M., Deng, J., Gersuk, V., Shalek, A. K., et al. (2015). MAST: a flexible statistical framework for assessing transcriptional changes and characterizing heterogeneity in single-cell RNA sequencing data. *Genome Biology*, 16:278.
- Gao, L. L., Bien, J., and Witten, D. (2022). Selective inference for hierarchical clustering. *Journal of the American Statistical Association*, 119(545):332–342.
- Gerard, D. (2020). Data-based RNA-seq simulations by binomial thinning. *BMC Bioinformatics*, 21:206.
- Gerard, D. and Stephens, M. (2020). Empirical Bayes shrinkage and false discovery rate estimation, allowing for unwanted variation. *Biostatistics*, 21(1):15–32.

- Gu, J., Wang, X., Halakivi-Clarke, L., Clarke, R., and Xuan, J. (2014). BADGE: a novel Bayesian model for accurate abundance quantification and differential analysis of RNA-Seq data. *BMC Bioinformatics*, 15:S6.
- Jabri, B. and Abadie, V. (2015). IL-15 functions as a danger signal to regulate tissue-resident T cells and tissue destruction. *Nature Reviews Immunology*, 15(12):771–783.
- Kang, G., Du, L., and Zhang, H. (2016). multiDE: a dimension reduced model based statistical method for differential expression analysis using RNA-sequencing data with multiple treatment conditions. *BMC Bioinformatics*, 17:248.
- Kruskal, W. H. and Wallis, W. A. (1952). Use of ranks in one-criterion variance analysis. *Journal of the American Statistical Association*, 47(260):583–621.
- Kuhn, J. A., Vainchtein, I. D., Braz, J., Hamel, K., Bernstein, M., Craik, V., et al. (2021). Regulatory T-cells inhibit microglia-induced pain hypersensitivity in female mice. *eLife*, 10:e69056.
- Law, C. W., Chen, Y., Shi, W., and Smyth, G. K. (2014). voom: precision weights unlock linear model analysis tools for RNA-seq read counts. *Genome Biology*, 15:R29.
- Leek, J. T. (2014). svaseq: removing batch effects and other unwanted noise from sequencing data. *Nucleic Acids Research*, 42(21):e161.
- Leek, J. T. and Storey, J. D. (2007). Capturing heterogeneity in gene expression studies by surrogate variable analysis. *PLoS Genetics*, 3(9):e161.
- Liao, Y., Wang, J., Jaehnig, E. J., Shi, Z., and Zhang, B. (2019). WebGestalt 2019: gene set analysis toolkit with revamped UIs and APIs. *Nucleic Acids Research*, 47(W1):W199–W205.
- Littman, D. R. and Rudensky, A. Y. (2010). Th17 and regulatory T cells in mediating and restraining inflammation. *Cell*, 140(6):845–858.
- Love, M. I., Huber, W., and Anders, S. (2014). Moderated estimation of fold change and dispersion for RNA-seq data with DESeq2. *Genome Biology*, 15:550.
- Lun, A. (2018). Overcoming systematic errors caused by log-transformation of normalized single-cell RNA sequencing data. *bioRxiv*.
- Lun, A. T. and Marioni, J. C. (2017). Overcoming confounding plate effects in differential expression analyses of single-cell rna-seq data. *Biostatistics*, 18(3):451–464.
- Lun, A. T. L., Chen, Y., and Smyth, G. K. (2016). It’s DE-licious: a recipe for differential expression analyses of RNA-seq experiments using quasi-likelihood methods in edgeR. In Mathé, E. and Davis, S., editors, *Statistical Genomics: Methods and Protocols*, pages 391–416.
- Lun, A. T. L. and Smyth, G. K. (2017). No counts, no variance: allowing for loss of degrees of freedom when assessing biological variability from RNA-seq data. *Statistical Applications in Genetics and Molecular Biology*, 16(2):83–93.
- Lund, S. P., Nettleton, D., McCarthy, D. J., and Smyth, G. K. (2012). Detecting differential expression in RNA-sequence data using quasi-likelihood with shrunken dispersion estimates. *Statistical Applications in Genetics and Molecular Biology*, 11(5).

- McCarthy, D. J., Chen, Y., and Smyth, G. K. (2012). Differential expression analysis of multifactor RNA-seq experiments with respect to biological variation. *Nucleic Acids Research*, 40(10):4288–4297.
- McCarthy, D. J. and Smyth, G. K. (2009). Testing significance relative to a fold-change threshold is a TREAT. *Bioinformatics*, 25(6):765–771.
- McDavid, A., Finak, G., and Yajima, M. (2021). MAST: model-based analysis of single cell transcriptomics. R package version 1.18.0.
- McGeachy, M. J., Chen, Y., Tato, C. M., Laurence, A., Joyce-Shaikh, B., Blumenschein, W. M., McClanahan, T. K., O’Shea, J. J., and Cua, D. J. (2009). The interleukin 23 receptor is essential for the terminal differentiation of interleukin 17-producing effector T helper cells in vivo. *Nature Immunology*, 10(3):314–324.
- Murphy, A. E. and Skene, N. G. (2022). A balanced measure shows superior performance of pseudobulk methods in single-cell RNA-sequencing analysis. *Nature Communications*, 13:7851.
- Okamura, H., Tsutsui, H., Komatsu, T., Yutsudo, M., Hakura, A., Tanimoto, T., et al. (1995). Cloning of a new cytokine that induces IFN- γ production by T cells. *Nature*, 378(6552):88–91.
- Phipson, B., Lee, S., Majewski, I. J., Alexander, W. S., and Smyth, G. K. (2016). Robust hyperparameter estimation protects against hypervariable genes and improves power to detect differential expression. *Annals of Applied Statistics*, 10(2):946–963.
- Pickrell, J. K., Marioni, J. C., Pai, A. A., Degner, J. F., Engelhardt, B. E., Nkadori, E., Veyrieras, J.-B., Stephens, M., Gilad, Y., and Pritchard, J. K. (2010). Understanding mechanisms underlying human gene expression variation with RNA sequencing. *Nature*, 464(7289):768–772.
- R Core Team (2021). R: a language and environment for statistical computing. R Foundation for Statistical Computing.
- Risso, D., Ngai, J., Speed, T. P., and Dudoit, S. (2014). Normalization of RNA-seq data using factor analysis of control genes or samples. *Nature Biotechnology*, 32(9):896–902.
- Ritchie, M. E., Phipson, B., Wu, D., Hu, Y., Law, C. W., Shi, W., and Smyth, G. K. (2015). limma powers differential expression analyses for RNA-sequencing and microarray studies. *Nucleic Acids Research*, 43(7):e47.
- Robinson, M. D., McCarthy, D. J., and Smyth, G. K. (2010). edgeR: a Bioconductor package for differential expression analysis of digital gene expression data. *Bioinformatics*, 26(1):139–140.
- Robinson, M. D. and Oshlack, A. (2010). A scaling normalization method for differential expression analysis of RNA-seq data. *Genome Biology*, 11:R25.
- Robinson, M. D. and Smyth, G. K. (2008). Small-sample estimation of negative binomial dispersion, with applications to SAGE data. *Biostatistics*, 9(2):321–332.
- Sarkar, A. and Stephens, M. (2021). Separating measurement and expression models clarifies confusion in single-cell RNA sequencing analysis. *Nature Genetics*, 53(6):770–777.

- Shimobayashi, M. and Hall, M. N. (2014). Making new contacts: the mTOR network in metabolism and signalling crosstalk. *Nature Reviews Molecular Cell Biology*, 15(3):155–162.
- Silva, A., Rothstein, S. J., McNicholas, P. D., and Subedi, S. (2019). A multivariate Poisson-log normal mixture model for clustering transcriptome sequencing data. *BMC Bioinformatics*, 20:394.
- Smyth, G. K. (2004). Linear models and empirical Bayes methods for assessing differential expression in microarray experiments. *Statistical Applications in Genetics and Molecular Biology*, 3(1).
- Soneson, C. (2014). `compcoder`—an R package for benchmarking differential expression methods for RNA-seq data. *Bioinformatics*, 30(17):2517–2518.
- Soneson, C. and Delorenzi, M. (2013). A comparison of methods for differential expression analysis of RNA-seq data. *BMC Bioinformatics*, 14:91.
- Soneson, C. and Robinson, M. D. (2018). Bias, robustness and scalability in single-cell differential expression analysis. *Nature Methods*, 15(4):255–261.
- Squair, J. W., Gautier, M., Kathe, C., Anderson, M. A., James, N. D., Hutson, T. H., et al. (2021). Confronting false discoveries in single-cell differential expression. *Nature Communications*, 12:5692.
- Stephens, M. (2017). False discovery rates: a new deal. *Biostatistics*, 18(2):275–294.
- Subedi, S. and Browne, R. P. (2020). A family of parsimonious mixtures of multivariate Poisson-lognormal distributions for clustering multivariate count data. *Stat*, 9(1):e310.
- The Gene Ontology Consortium (2020). The Gene Ontology resource: enriching a GOld mine. *Nucleic Acids Research*, 49(D1):D325–D334.
- Townes, F. W., Hicks, S. C., Aryee, M. J., and Irizarry, R. A. (2019). Feature selection and dimension reduction for single-cell RNA-Seq based on a multinomial model. *Genome Biology*, 20:295.
- Townes, F. W. and Street, K. (2021). *glmpca: dimension reduction of non-normally distributed data*. R package version 0.2.0.9000.
- Urbut, S. (2017). *Flexible statistical methods for jointly modeling effects*. PhD thesis, University of Chicago, Chicago, IL.
- Urbut, S. M., Wang, G., Carbonetto, P., and Stephens, M. (2019). Flexible statistical methods for estimating and testing effects in genomic studies with multiple conditions. *Nature Genetics*, 51(1):187–195.
- Wang, T., Li, B., Nelson, C. E., and Nabavi, S. (2019). Comparative analysis of differential gene expression analysis tools for single-cell RNA sequencing data. *BMC bioinformatics*, 20:40.
- Wang, W. and Stephens, M. (2021). Empirical Bayes matrix factorization. *Journal of Machine Learning Research*, 22(120):1–40.

- Wang, Z., Gerstein, M., and Snyder, M. (2009). RNA-Seq: a revolutionary tool for transcriptomics. *Nature Reviews Genetics*, 10(1):57–63.
- Wei, Y., Tenzen, T., and Ji, H. (2015). Joint analysis of differential gene expression in multiple studies using correlation motifs. *Biostatistics*, 16(1):31–46.
- Willwerscheid, J. (2021). *Empirical Bayes matrix factorization: methods and applications*. PhD thesis, University of Chicago, Chicago, IL.
- Wojno, E. D. T., Hunter, C. A., and Stumhofer, J. S. (2019). The immunobiology of the interleukin-12 family: room for discovery. *Immunity*, 50(4):851–870.
- Yoshimoto, T., Okamura, H., Tagawa, Y.-I., Iwakura, Y., and Nakanishi, K. (1997). Interleukin 18 together with interleukin 12 inhibits IgE production by induction of interferon- γ production from activated B cells. *Proceedings of the National Academy of Sciences*, 94(8):3948–3953.
- Zhang, M., Liu, S., Miao, Z., Han, F., Gottardo, R., and Sun, W. (2022). IDEAS: individual level differential expression analysis for single-cell RNA-seq data. *Genome Biology*, 23:33.
- Zheng, G. X., Terry, J. M., Belgrader, P., Ryvkin, P., Bent, Z. W., Wilson, R., et al. (2017). Massively parallel digital transcriptional profiling of single cells. *Nature Communications*, 8:14049.
- Zhu, A., Ibrahim, J. G., and Love, M. I. (2019). Heavy-tailed prior distributions for sequence count data: removing the noise and preserving large differences. *Bioinformatics*, 35(12):2084–2092.
- Zhu, J., Guo, L., Min, B., Watson, C. J., Hu-Li, J., Young, H. A., Tschlis, P. N., and Paul, W. E. (2002). Growth factor independent-1 induced by IL-4 regulates Th2 cell proliferation. *Immunity*, 16(5):733–744.
- Zou, Y. (2021). *Bayesian variable selection from summary data, with application to joint fine-mapping of multiple traits*. PhD thesis, University of Chicago, Chicago, IL.